Controlled Deformation of Light Activated Polymers

A Thesis Submitted to the Faculty of

The University of Colorado

by

Jennifer Ryu

B.S., Georgia Tech, 2010

in partial fulfillment of the requirements for the degree of

Master of Science

Department of Mechanical Engineering

December 2012

This thesis entitled:

Controlled Deformation of Light Activated Polymers

written by Jennifer Ryu

has been approved by the Department of Mechanical Engineering

_____

Jerry Qi, PhD

_____

Yifu Ding, PhD

Date _____

The final copy of this thesis has been examined by the signatories, and we find that both the content and the form meet acceptable presentation standards of scholarly work in the above mentioned discipline.

Abstract

Ryu, Jennifer (M.S. Mechanical Engineering)

Controlled Deformation of Light Activated Polymers

Thesis directed by Dr. Jerry Qi and Dr. Martin Dunn

The motivation for this research was to demonstrate the ability to program the deformation of light activated polymers (LAPs) by controlling the chemical makeup, the mechanical parameters of the test, and the optical stimulus. The deformation of LAPs is a product of the network reformation that occurs due to the initiation of the Radical-Mediated Additional Fragmentation Chain Transfer (RAFT) mechanism. The RAFT mechanism minimizes the free energy present in the system, which can result in a localized plastic deformation under certain experimental parameters.

Tests were done to demonstrate the ability of controlled surface patterning and out of plane bending by manipulating this RAFT mechanism. Surface patterning was exhibited by initiating the RAFT mechanism in localized regions of an optically thin sample under some strain. To demonstrate bending, “optically thick” samples were used to create a gradient of network reformation, and thereby curvature. In addition to creating deformation, the objective of this work included predicting and prescribing surface features through control and modification of the testing parameters. To assist in this work, an FEA model was constructed in ABAQUS that effectively predicted the deformation caused by imposed values of applied strain, region of irradiation and maximum stress relaxation potential.

This study showed that by sufficiently characterizing the network rearrangement of optically thin and optically thin photoactive polymers, the deformation behavior could be predicted and controlled. In the optically thin case, this translates into precise control of surface patterning through

the use of physical masks to define irradiation zones. In the optically thick case, tests illustrated that by using multiple prescribed irradiation steps based on the characterization studies, appropriate testing procedures could be defined to create bending out of plane. This work ultimately demonstrated the versatility of the deformation possible in LAPs.

Acknowledgements

For this work, I would like to thank my advisors, Dr. Martin Dunn and Dr. Jerry Qi for the opportunity to work with them and their guidance during the course of the project.

I would also like to thank my committee members, Dr. Yifu Ding and Dr. Robert McLeod, for their insight and for offering different perspectives for the project at hand.

Additionally, I would like to thank Dr. Christopher Bowman's research group, as well as Dr. Robert McLeod's research group for their help designing an effective experimental setup.

Table of Contents

List of Tables

List of Figures

1. Introduction

1.1 Environmentally –Activated Polymers

Studying the mechanical properties and mechanical responses of materials that are environmentally or naturally actuated is currently of interest because of their potential to revolutionize biomedical design, microelectronics, as well as renewable energy systems design. Typical environmental stimuli for these materials include: thermal stimuli, mechanical load, and optical stimuli. Light-activated materials have the advantage over thermal and mechanical stimulated materials because wavelengths of light have a higher are more easily controlled than the temperature of the material, and they have the added benefit of actuation from a distance without any physical contact. With either a thermal or mechanical stimulus, it is also more difficult to isolate a localized region to actuate. Additionally, given absorbance and reaction pathways with different energy levels can create both negative and positive photoresists, which means the material can be polymerized or depolymerized with different wavelengths of light. With this additional control, the properties of the material in localized areas can be prescribed into a much more complex pattern to a higher degree of precision than would be otherwise obtained using thermal or mechanical stimuli.

1.2 Programmable Matter

Programmable matter refers to a group of materials in which the shape or stiffness of the material can be activated when given a particular stimulus in order to perform the desired function [1]. Examples of programmable matter include materials that exhibit the shape memory effect, are temperature responsive, self-healing materials and photo-mechanical systems, or some subset of those properties. The material studied for the remainder of this report is a photo-mechanical polymer system that undergoes radical addition fragmentation chain transfer to break and reform bonds in energetically

favorable states [2]. Other types of programmable matter include: shape memory alloys, shape memory polymers, and material that can recover stress with time. The most common stimulus for programmable matter is a change in temperature, as is the case for most shape memory systems.

Programmable matter is particularly common in the biomedical and MEMS applications. In the biomedical field, the shape memory effect is a common solution to minimally invasive implantation of devices such as arterial stents. For this particular application, Nitinol is a common choice of material because of its shape memory behavior and its superelasticity [3], [4], [5]. However, as a metal, Nitinol has poor biocompatibility due to the wear products created during corrosion [6], [7]. In the MEMS field, the shape memory response can be used to develop a type of actuator [8]. For this application, a programmable material can be used to create components that assemble into their appropriate positions in response to the thermal stimulus.

1.3 Types of Programmable LAPs

Light-activated polymers (LAPs) are crosslinked network polymers that absorb irradiation at specific wavelengths and exhibit a desired response [9]. The optical stimulus can be used to initiate the cleavage of a photointiator or cause the cleavage of photoreversible crosslinks present in the polymer network. The LAP response differs between polymeric species and these responses create materials with unique optical and mechanical properties [10],[11].

Liquid Crystal Elastomers (LCEs) are a type of LAP commonly used in electronic displays. These polymers consist of networks that exist in the rubbery regime, while maintaining localized regions of crystallinity. Through controlled irradiation, Corbett et al. have demonstrated that these LCEs can be photoisomerized to alter the properties of the internal network [12]. This results in both the generation of new optical properties by changing the diffraction of light as well as mechanical deformation in the

irradiated regions [13]. The molecules within the elastomer go from the ground state, the linear *trans*- state to an excited, bent, *cis*- state. This naturally causes light to react differently through these deformed regions [14].

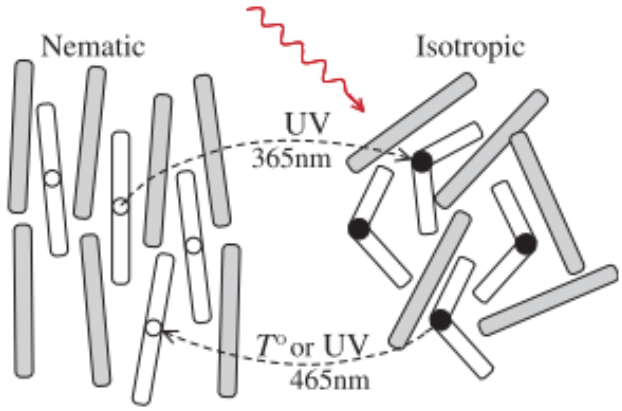

Figure 1. Light-induced deformation from the trans- to cis- state of LCEs [12]

Cinnamic polymers have been used to demonstrate the ability to use light to induce a shape memory effect as well as a shape change effect [15]. Shape changing gels respond to an optical stimulus and continue to respond as long as the stimulus is applied. Shape memory polymers (SMP) can be programmed to revert to a specific, permanent geometry when an appropriate stimulus is applied. This is done through the use of tunable photoreversible crosslinks, which can be formed "fix" a new, deformed configuration, or cleaved to return to the original network configuration.

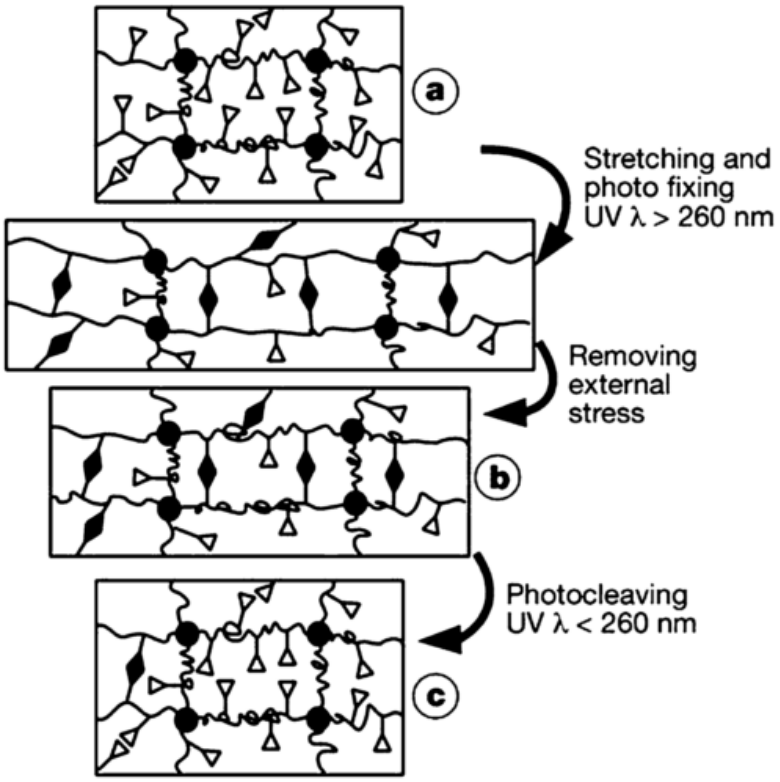

Figure 2. Photoreversible crosslinks used to "fix" a deformed configuration in a cinnamic polymer [15]

Thiol-ene polymers have also been engineered to be photoresponsive, by way of integrating photoinitiators into the network and utilizing the RAFT mechanism, which will be discussed later. These networks include embedded molecules, photoinitiators that are photoresponsive at particular wavelengths. Upon homolytic cleavage of these molecules, radicals form and initiate cleavage and reformation of the polymer backbone [16].

1.4 Advantages of LAPs

LAPs have advantages over other types of programmable matter due to their versatility and method of actuation. Characteristics that LAPs exhibit that provide an advantage over other programmable

matter include: more freedom to modify the chemical structure, actuation at a distance, the ability to prescribe precise deformation, and the ability to increase the flaw tolerance of a material.

In the biomedical field, Shape Memory Alloys (SMAs) like Nitinol are commonly implemented for use as arterial stents because of their superelasticity and thermally actuated shape memory effect [3]. However, use of a smooth metallic material as a biomaterial is a poor choice because of its surface properties as well as its mechanical properties. Without any coating, metals do not have the proper surface receptors to encourage integration into the biological environment. Also, the lack of texture prevents endothelial cells from adhering to the implant and encapsulating the material [6]. Since metallic materials corrode over time, without an encapsulating layer, the wear and corrosion particles will be easily released into the blood stream causing an undesirable immune response [6]. Metallic materials also naturally have a much higher elastic modulus than that of the vascular tissue. This dissimilarity leads to a mismatch in stress distribution during fatigue loading caused by blood flow and poor integration. An additional concern for nickel-based materials is the risk of sensitizing the host and causing an adverse allergic reaction. In this application, a polymeric material with similar deformation behavior can be easily chemically modified to have desirable surface characteristics [17]. The elastic modulus can also be carefully prescribed by controlling the crosslink density of the network. With polymeric systems, there is more flexibility in the chemical structure of the implant, guarding against potential carcinogens leaching into the body, as is common with metallic implants. LAPs can be modified to meet these requirements of biocompatibility and would be a suitable alternative for this application.

LAPs also have the advantage over thermally actuated SMAs and SMPs of having highly tunable deformation. This is an advantage in both biomedical and Micro Electronic Mechanical Systems (MEMS) applications. In SMAs and SMPs, the material can “save” or “remember” only one or two deformed shapes. Since these systems are typically thermally actuated, these deformed patterns are realized at

specific temperatures. For biomedical applications, the body temperature is used to actuate the material into its "permanent," predefined shape. MEMS devices are typically shipped in a manner so that the components are not in their functional positions to prevent damage and breaking of parts. A thermal stimulus is applied to align components of the system after delivery. Both of these cases require preexisting knowledge about the surrounding environment, and have no room for error because of the inability to modify the deformation *in situ*. Because the deformation in LAPs is caused by photons cleaving bonds, the deformation can be modulated by controlling the duration and dose of the irradiation and therefore require no prior knowledge or preprogramming to assume an appropriate shape. The highly tunable deformation also applies to regions of deformation. LAPs can be modified in distinct regions by "masking" regions and preventing any photons from hitting those areas and causing deformation. In this manner, specific areas can be targeted to create complex deformation behavior.

LAPs have also been shown to increase flaw tolerance and improve shrinkage stress [18], [19]. These characteristics have implications in the biomedical and renewable energy fields. Photocured acrylate systems are widely used in the dental industry because they are bioinert and closely mimic the properties of natural teeth. However, these polymers shrink during curing and cause residual stress and stress concentrations that lead to microcracks and premature failure of the implant [19]. In the renewable energy field, solar energy harvesting typically requires tracking to optimize output of PV cells. However, thin film Si can be deformed into troughs to concentrate the light and minimize the need for tracking, while optimizing output [20]. Deformation of the thin film into these 3D structures will inevitably lead to some impurities and residual stresses in the material. Long et al. showed that in LAPs, if a defect or stress concentration forms, additional irradiation can reduce that stress, leading to higher crack propagation resistance and a longer lifetime of the material [18].

Previous work with LAPs

Previous work has been done to investigate the stress relaxation behavior caused by network reformation as well as the manipulation of the stress relaxation to induce deformation behavior. Scott et al. used a photoactive polymer system with embedded photoinitiators to cause radical-mediated network reformation [9]. In this network, photons at appropriate wavelengths cause homolysis of the photoinitiators, which cleave and reform bonds in the polymer network. They investigated the effect of varying the intensity of irradiation on the rate of stress relaxation in the sample. They confirmed that with increasing intensity, the rate of stress relaxation increases as well, as a result of the increase in the amount of photons hitting the surface at any given moment.

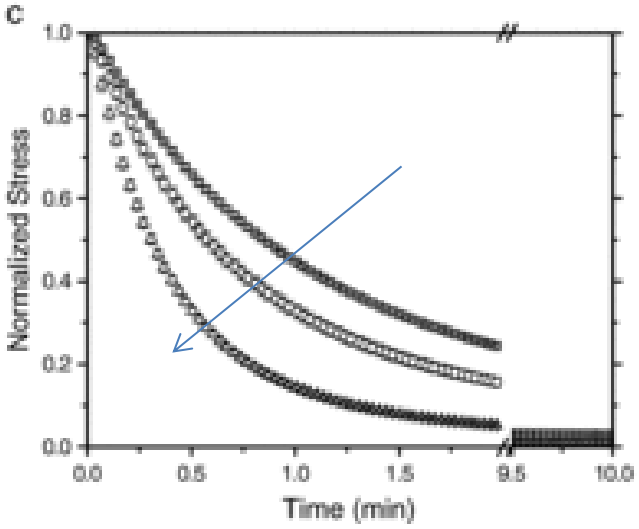

Figure 3. Previous study performed to study the effect of intensity on the rate of stress relaxation in a LAP system, with the arrow in the direction of increasing intensity [21].

To examine the effect of the network reformation on the macroscopic structure, the material was subjected to biaxial strain and then irradiated through a physical photomask. The subsequent deformation was approximately consistent with the mask used to create the deformation, and the

change in depth of the irradiated regions was measured. However, this work did not show any attempt to characterize the deformation behavior or predict and prescribe surface patterns.

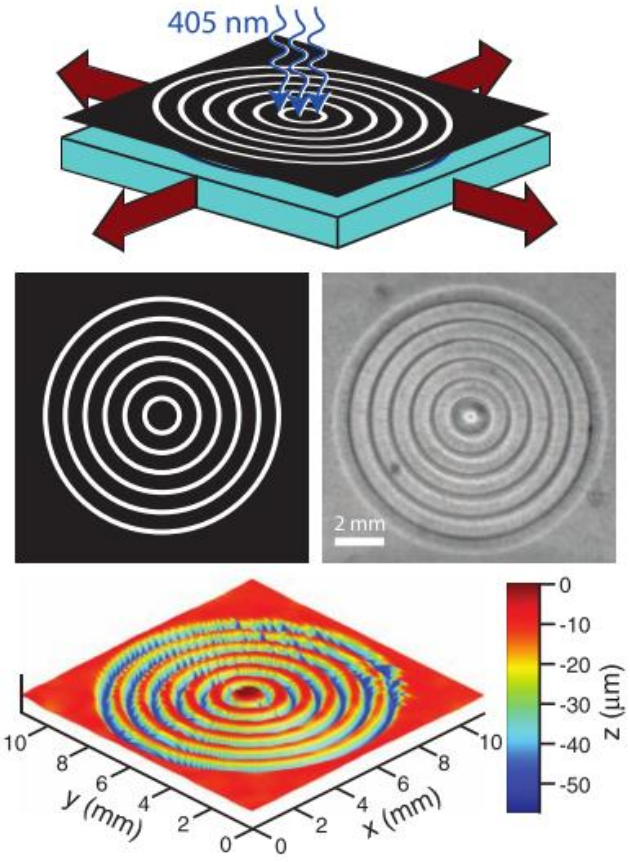

Figure 4. Scott et al. created deformation by applying biaxial strain and irradiating the sample through a physical photomask. The subsequent deformation was measured using a Zygo white light optical profilometer [21]**.**

Scott et al. further investigated the stress relaxation behavior of the material by embedding a UV photoabsorber to create attenuation of light and therefore non-uniform network reformation. The addition of the photoabsorber controls the light penetration through the thickness of these samples, and the subsequent stress relaxation gradient induces a curvature in the material [9], [22]. The following figure shows a material with varying degrees of induced deformation. This result was caused by controlling the concentration of photoabsorber embedded in the system that altered the light penetration in the sample. Even with embedded photoabsorbers, given a high enough intensity and long

enough period of time, the light should be able to eventually activate all of the photoinitiators in the system, reducing the potential for curvature. However, these samples were irradiated for a short period of time (15 sec), which aided in created a large difference in deformation between the front and the back of the sample, resulting in a high degree of curvature.

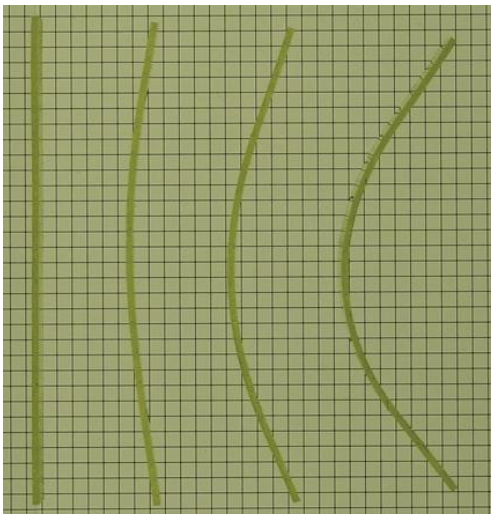

Figure 5. Work done by Scott et al. to induce curvature by increasing the concentration of UV photoabsorber embedded in the system[22]

Previous work has been done modeling the curvature induced by varying intensity, time and strain, given an absorptivity of a system. The following figures present the theoretical prediction for the curvature induced in a material with a known absorptivity and thickness by modifying the parameters of intensity, time, and applied strain [2]. These simulations assume that the initiators can diffuse through the sample, resulting in a difference in stress relaxation between the front and back of the sample, regardless of how many photons hit the sample.

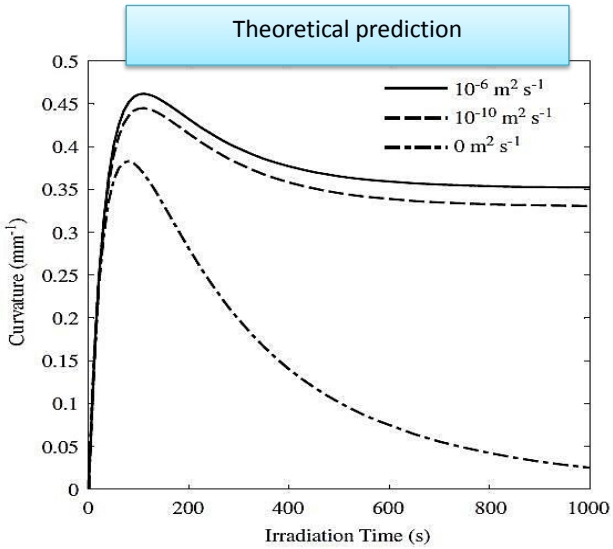

Figure 6. Theoretical prediction for the resulting curvature as a function of irradiation time (s) [2]

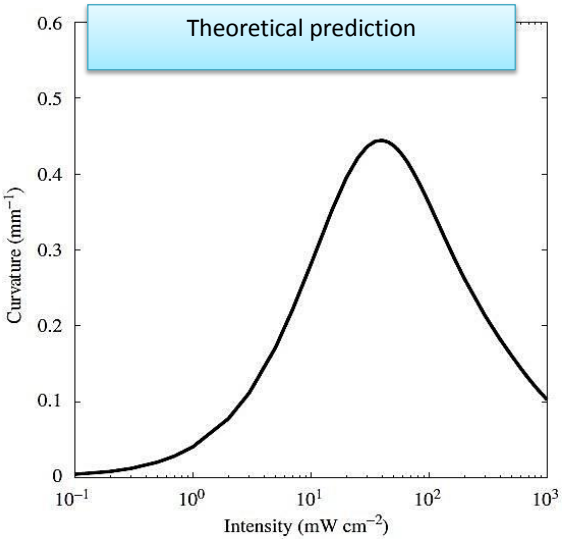

Figure 7. Theoretical prediction for the resulting curvature as a function of irradiation intensity (mW/cm^2) [2]

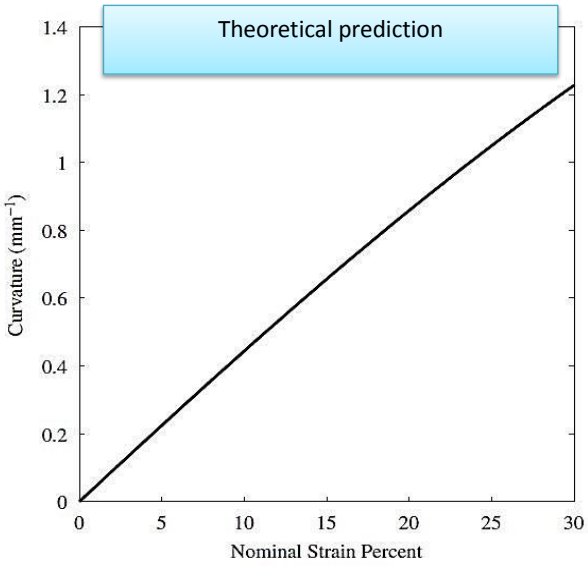

Figure 8. Theoretical prediction for the resulting curvature as a function of the nominal strain percent [2]

2. Radical-Mediated Additiol Fragmentation Chain Transfer (RAFT) Mechanism

The Radical-Mediated Addition Fragmentation Chain Transfer (RAFT) mechanism is a method to utilized free radicals to induce network reformation. This mechanism can be initiated in light-actuated systems through the activation of photoinitiators through reactions with photons of appropriate wavelength and the subsequent degradation of the photoinitiators into free radicals. In an allyl sulfide group, these radicals break the C-C double bond, which creates an unstable radical. The termination of this radical results in a reformed network in a lower energy states as well as another thiol radical that can continue to cleave and reform the polymer backbone [23–27].

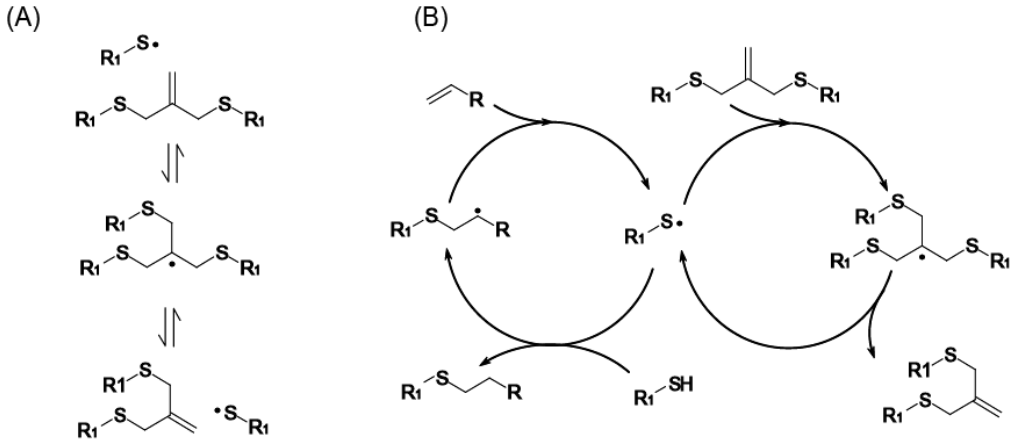

Figure 9. (A) Thiol radical attacking the C-C double bond and causing an unstable on the middle carbon, resulting in network reformation upon stabilization (B) Schematic of the pathways for the vinyl ether and the allyl sulfide functionalities with the radical [19]

Since the RAFT mechanism will reform the polymer network in the lowest available free energy state, when the network is irradiated under some applied strain, it will relax some of the stress present in the system. When the sample is released from the applied strain, because of the stress relaxation, it will retain some of the deformed state resulting in permanent deformation [2].

3. Materials & Equipment

3.1 Monomers

The three functionalities of interest in this study were: thiols, vinyl ethers, and allyl sulfides. Three distinct monomers units were used in this study including: ethylene glycol dimethyl propionate (EGDMP), pentaerythriol tetra(3-mercaptopropionate) (PETMP), and 2-methylene-propane-1,3- di (thioethyl vinylether) (MDTVE).

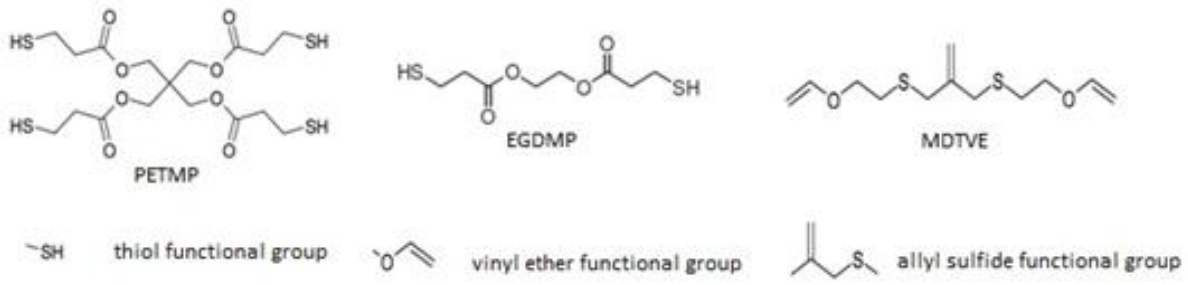

Figure 10. Monomer units used to create the network copolymer

Pentaerythriytol tetrakis(3-mercaptopropionate), CAS-No. 7575-23-7 (PETMP) is a tetrafunctional monomer with four thiol functionalities and was purchased from Sigma-Aldrich®. The chemical structure is presented in Figure 10, with the relevant functional groups labeled. The material has the appearance of a colorless, viscous liquid, and has minimal light absorbance properties. The molecular weight of this monomer unit is 488.66 g/mol. The boiling point of the monomer is 275°C at 1 mmHg pressure and the flash point is >110°C. The density is 1.28 g/cm^3 at 25°C [28].

Ethylene glycol dimethyl propionate, CAS-No. 22504-50-3 (EGDMP) is a linear, di-thiol monomer unit, and was purchased from Evans Chemetics. The chemical structure of the monomer is presented in Figure 10, with the relevant functional groups labeled. The molecular weight of this monomer is 238.32

g/mol and has a density of 1.218 g/cm^3. The boiling opint is 358.7°C at 760 mmHg pressure and has a flashpoint of 255.6°C [29].

The final monomer, 2-methylene-propane-1,3- di (thioethyl vinylether) (MDTVE) is a slightly yellow solution with a chemical structure presented in Figure 10. There is no Material Safety Data Sheet, because the monomer was synthesized by the Bowman Research Group in the CU Chemical Engineering Department following the procedure given by Evans et al., and previously described in literature [30].

3.2 Photoinitiators and Photoabsorbers

All of the units that were embedded into the system were obtained from BASF (formerly CIBA). Irgacure 819 (Bis(2,4,6-trimethylbenzoyl)-phenylphosphineoxide–BPO) photoinitiator activated using UV and visible light. It is a yellow powder with a molecular weight of 418.5 g/mol and a melting point between 127-133°C. The chemical structure of the material is given in

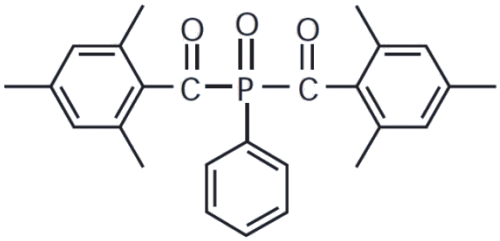

Figure 11. Chemical structure of Irgacure 819 [31]

The solubility of the powder at 20°C (g/100 g solution) is provided in Table 1.

Table 1. Solubility (g/100g solution) for Ciba Irgacure 819 at 20 C [31]

Solvent	Solubility (g/100 g solution)
Acetone	14
Butylacetate	6
Methanol	3
Toluene	22

Heanedioldiacrylate (HDDA)	9
Oligomeric Acrylate	3

The following figure shows the extinction curve for Irgacure 819, which indicates the ability of the molecule to absorb photons of a given wavelength and degrade into two radical species.

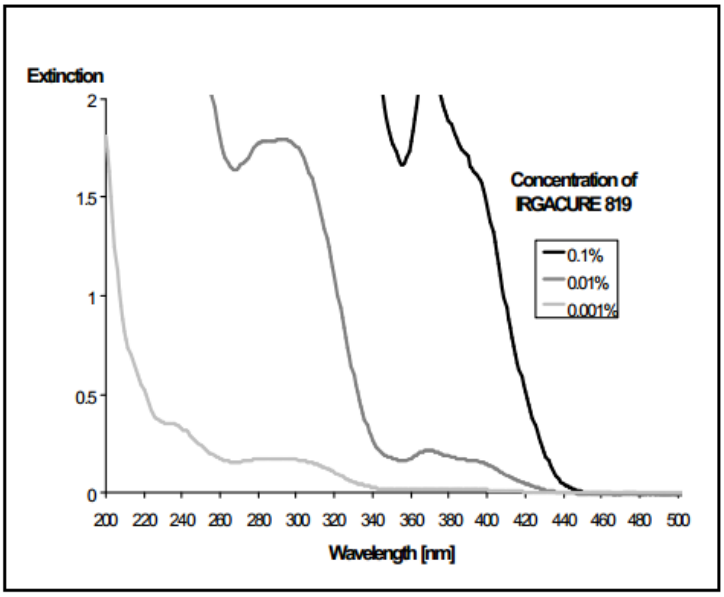

Figure 12. Absorbance Spectra for different concentrations Irgacure 819 dissolved in acetonitrile [31]

The multiple curves in the figure indicate that higher concentrations of Irgacure 819 shift the extinction curve to the right. For a concentration of 1 wt%, the extinction curve should lie mostly in the visible region.

Irgacure 184 (1-Hydroxy-cyclohexyl-phenyl-ketone) is a highly efficient photoinitiator that has the appearance of an off-white crystalline powder. The molecular weight is 204.3 g/mol and the melting point is between 45-49°C. The chemical structure is presented in Figure 13 [32].

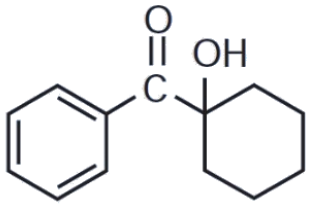

Figure 13. Chemical composition for the photoinitiator Irgacure 184 [32]

The solubility of Irgacure 184 in different solvents is presented in Table 2.

Table 2. Solubility (g/100 g solution) for Irgacure 184 at 20C in multiple solvents [32]

Solvent	Solubility (g/100 g solution)
Acetone	>50
Butylacetate	>50
Methanol	>50
Toluene	>50
Hexanedioldiacrylate (HDDA)	>50
Oligomeric Triacrylate	~40
Trimethylolpropanetrisacrylate (TMPTA)	43
Triporpyleneglycoldiacrylate (TPGDA)	43

The absorbance curve describes the ability of a molecule to absorb light at different wavelengths. The absorbance curve for Irgacure 184 at different concentrations in acetonitrile is given in Figure 14.

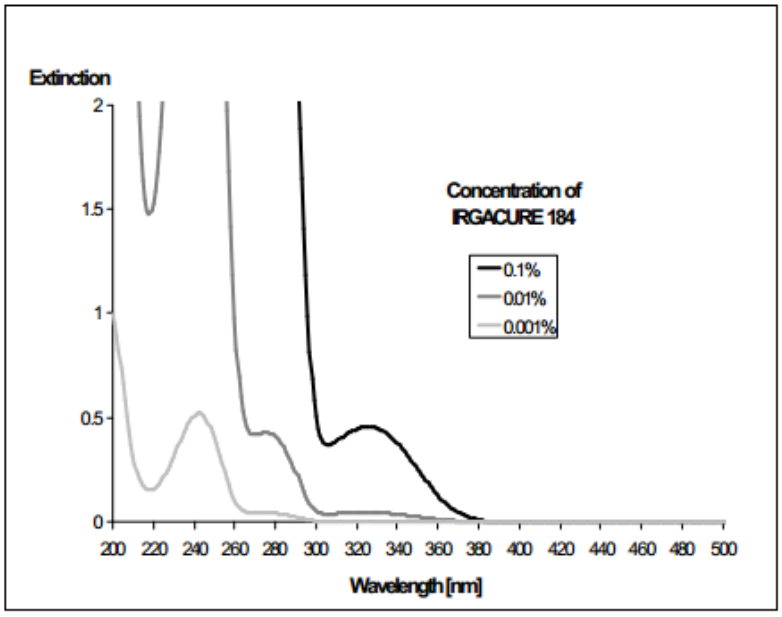

Figure 14. Absorbance Spectra for different concentrations for Ciba Irgacure 184 in acetonitrile

Tinuvin 5060 has the appearance of a viscous amber liquid and is a liquid light stabilizer that can absorb some measure of inicident light. The dynamic viscosity at 20°C is 10,000 mPa·s and the density at 20°C is 0.98 g/mL. The chemical structure and molecular weight were not provided in the MSDS by Ciba. The UV transmittance spectrum for a 1 cm cell thickness sample of a toluene solution with a mass concentration of 40 mg/L is presented in Figure 15 [33].

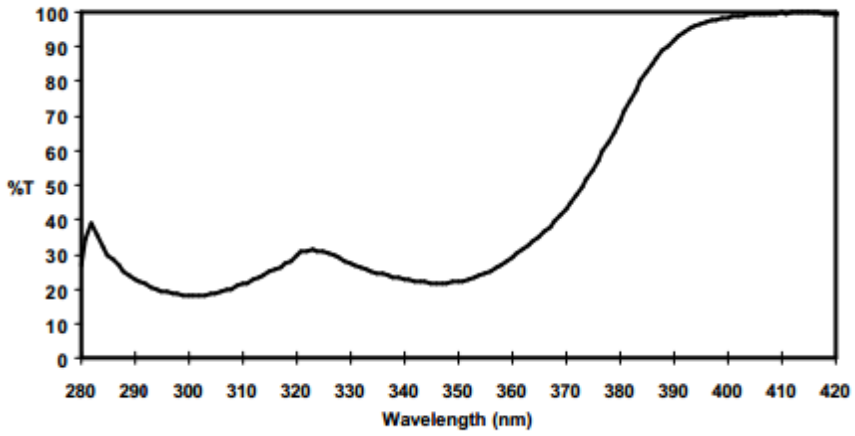

Figure 15. UV Transmittance Spectrum for 1cm cell thickness sample of Ciba Tinuvin 460 in a 40g/L toluene solution [33]

Tinuvin 460 is a light stabilizer of the hydroxyphenyl-triazine class with the appearance of a slightly yellow powder. The absorbance spectrum for Tinuvin 460 is given in Figure 16. The chemical structure, molecular weight, and solubility were not available on the material data sheet provided by BASF/Ciba.

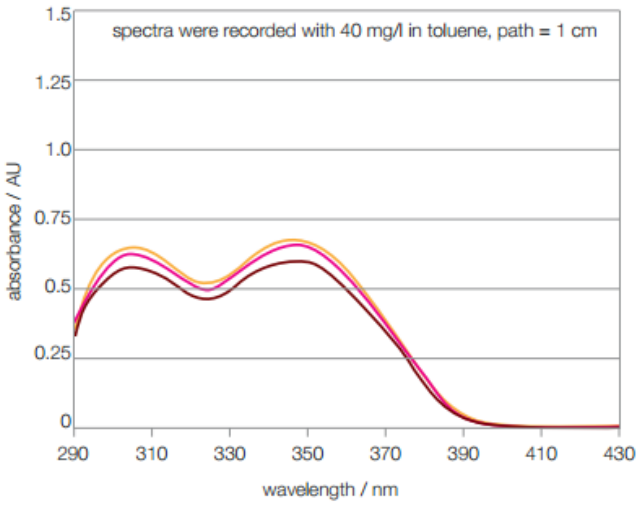

Figure 16. Absorbance Spectra for the Tinuvin 400-series of light stabilizers in a 40 mg/L toluene solution and a path length of 1 cm [34]

3.3 Light Curing System

The light source used in the following experiments was the Omnicure® S2000 purchased from Lumen Dynamics Group Inc. The S2000 is a precisions spot UV curing system with closed loop feedback with a high pressure 200 Watt Mercury vapor short arc lamp. The filter used on the light source was the standard 320-500 nm filter. The power output as a function of wavelength is given in Figure 17.

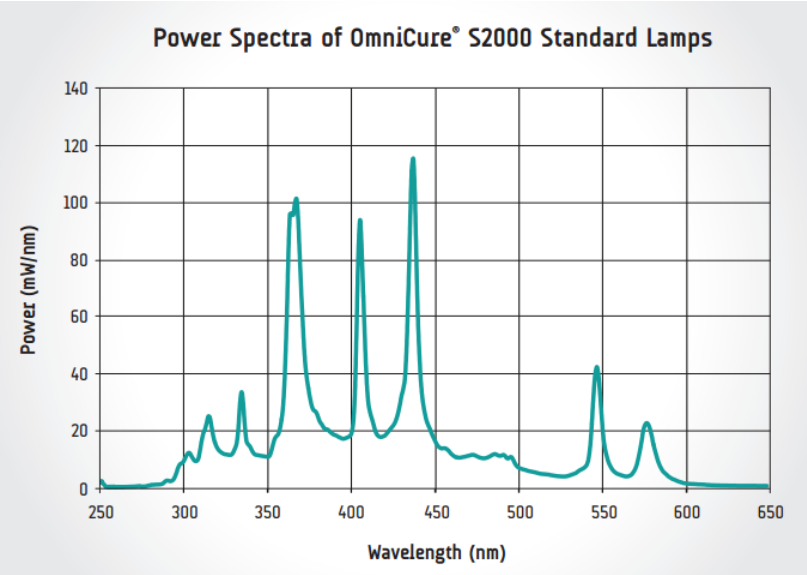

Figure 17. Power Spectra curve for the OmniCure S2000 lamp wtih the standard 320-500 nm filter [35]

The light guide used in conjunction with the S2000 was the Omnicure® liquid light guide with an 8mm tip diameter. The 8 mm Omnicure® adjustable collimating adaptor was placed on the end of the light guide to create a spot with approximately even light distribution throughout the spot. An iris diaphragm with a 42 mm outer diameter was purchased from Edmund Optics to further control the light source. This diaphragm had 10 leaves which allowed for a maximum aperture of 42.6 mm and a minimum aperture of 1.2 mm. In order to measure the light intensity given by the S2000 lamp, the ILT1400A radiometer/photometer and the XRL340A detector were purchased from International Light

Technologies Inc. The radiometer has a measurement range from 100 picoAmps to 350 microAmps with a display resolution of 10 picoAmps, has a linearity of 0.2%, and has a refresh rate of 0.5 s. The XRL340A is an attenuated photoresist detector that can measure wavelengths from ~320nm-500nm. The typical response curve is presented in Figure 18.

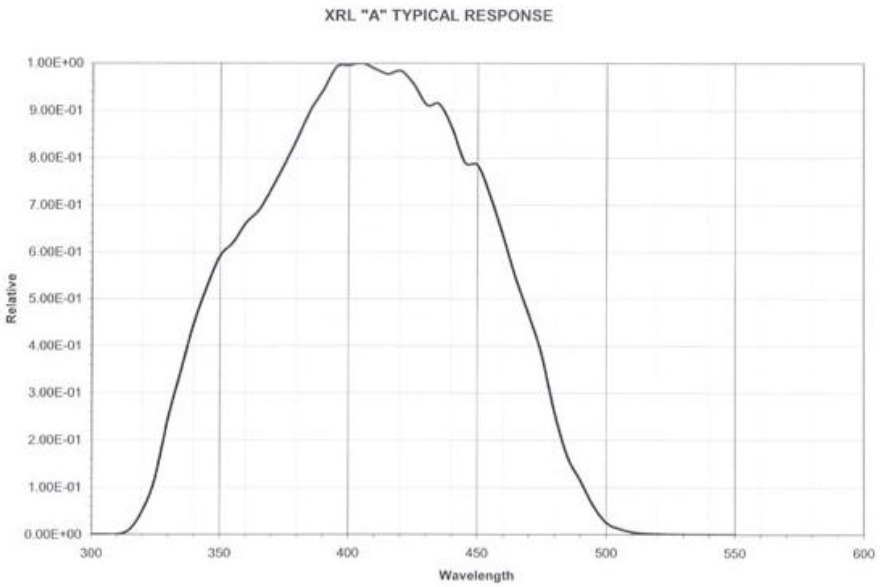

Figure 18. Typical response curve for the International Light Technologies XRL340A photoresist detector [36]

Additionally, bandpass filters at 365 nm with a 10 nm bandwidth and 400-500 nm with were purchased from Edmund Optics to control the wavelength of the incident irradiation.

3.4 Stage Strain Tester

To create a mechanical tester with precise, two 12 mm square aluminum linear ball bearing stages with micrometer position control from Edmund Optics were mounted to a stage. These stages were outfitted with aluminum plates that could be tightened using a thumb screw that acted as grips to hold testing samples.

3.5 DMA Q800

The mechanical tester used in the following experiments was the TA Instruments Q800 Dynamic Mechanical Analyzer with the tension grips. The maximum force of this machine is 18 N and the minimum force is 0.001 N with a resolution of 0.0001N. The strain resolution is 1 nm and the modulus range is 10^4 to 3 x 10^{12} Pa with a precision of +/- 1% [37].

3.6 Veeco Dektak 6M Stylus Surface Profilometer

The Dektak 6M Stylus Surface Profilometer from Dymek Company Ltd is a semi-manual instrument that provides data on the surface profile of a material by dragging a stylus along a sample and measuring the vertical deflection of the stylus tip, which has a diameter of 1.2 microns. The force provided by the stylus is programmable down to 1 milligram and has a maximum deflection of +/- 1 mm in the Z-height direction. The rate of scanning can be set by the user and this rate determines the resolution of the data in the direction of the scan [38].

4. Methods

4.1 Sample Preparation

To ensure complete polymerization of the sample, a 16:15 ratio of the thiol:vinyl ether functional groups was used. A slight excess of thiol was used to ensure complete conversion of the vinyl ether functional group because small proportion of the thiol undergoes a side reaction with the allyl sulfide during the polymerization step. The monomers were mixed in three different stoichiometric ratios to examine the effect of crosslinking density of the polymer network. Both PETMP and EGDMP contain only thiol functionalities, however, since PETMP is tetrafunctional, reacting more of the vinyl ether groups to the thiol groups contained within the PETMP will increase the crosslink density of the network. The three PETMP/MDTVE/EGDMP stoichiometric ratios used were, in the order of decreasing crosslink density: 2/5/3, 1/5/4, and 0.5/5/4.5. The photoinitiators used in the system were: Irgacure 819 for the FRP under visible light and Irgacure 184 for the network reformation under UV irradiation. These phototinitiators were chosen because of their ability to absorb certain wavelengths and bonds present within the molecule that cleave homolytically given photons of sufficient energy. The appropriate weights for each of the monomers were added to a small glass vial, then the 1 wt% of both of the two photoinitiators (Irgacure 184, and Irgacure 819) were added to the solution. This solution was mixed using a vortex for 2 minutes to aid in the dissolution of the photointiator particles. For the optically thick samples, 1 wt% of the Tinuvin 460 or 3 wt% of the Tinuvin 5060 was then added to the system, and the system was mixed for an additional 15 seconds. Two borosilicate glass slides of dimensions 50 mm x 75 mm were cleaned with methanol, coated with a hydrophobic layer (Rain-X) and separated by plastic shims with a thickness of 152 microns. The ends of the slides were clipped together with binder clips, so the unreacted monomer solution could be injected into the space between the two slides using a syringe and needle. The vinyl ether is very unstable and any ambient light will activate the

photoinitiators and initiate the polymerization of the gel. As such, the solution was mixed and carefully inserted into the glass slides quickly after the addition of the MDTVE before the gel becomes too viscous to inject. While the injection must be done quickly enough that the solution remains fluid enough to inject into a 152 micron space, the injection must also be done slowly enough to prevent air bubbles from creating air holes in the polymer sheet. The solution was irradiated using the Omnicure arc S2000 lamp at 40 mW/cm^2 with a 400-500 nm bandpass filter for 30 min. The intensity of the incident irradiation was measured using the International Light ITLL1400A spectrophotometer with the XRL340A detector. The bandpass filters allow some amount of near UV through; however, the borosilicate glass absorbs light at 365 nm, allowing much of the 184 to remain unreacted.

Figure 19. Injection of the unreacted monomer solution into the space between glass slides

After the curing of the sample, a razor was inserted between the plastic shim and one of the glass slides to gently pry the glass slides apart without tearing the thin film sample. After one of the glass slides was removed, the plastic shims were cut off. The polymer sheet was then cut into 20 mm x 4 mm samples using a metal die of appropriate dimensions. These samples were carefully removed from the slides using a razor blade and placed in the appropriate mechanical tester.

4.2 DMA Stress Relaxation

The first test on all the samples was a stress relaxation test to determine the maximum potential of the material to reform its network by measuring the residual stress. The procedure was similar to that of a typical stress relaxation test performed on polymers, however, the stress reduction in this case is a result of the network reformation rather than the viscoelasticity of the polymer sample. To measure the total volume fraction of the sample that could completely relieve the stress in the material, stress relaxation tests were performed in the DMA Q800 in a dark room, where the only light sources were the Omnicure mercury arc lamp and the computer screen. The samples were taped on the ends to create "tabs" that aided in handling the material, and then placed in the DMA. The samples were held at zero train for 2 minutes and then strained at a rate of 0.005 min^{-1} to a maximum strain. The maximum strains studied were: 3.5%, 4.5%, 6.0%, 7.5%, and 10%. This strain was held for 2 minutes. The sample was then irradiated for 15 minutes at constant strain. The sample was held at the final strain for an additional 5 minutes in the absence of light to eliminate any thermal effects. An additional 5% strain was applied to the sample to compare the post-irradiation modulus to the original modulus to compare the crosslink density and provide information about the network reformation.

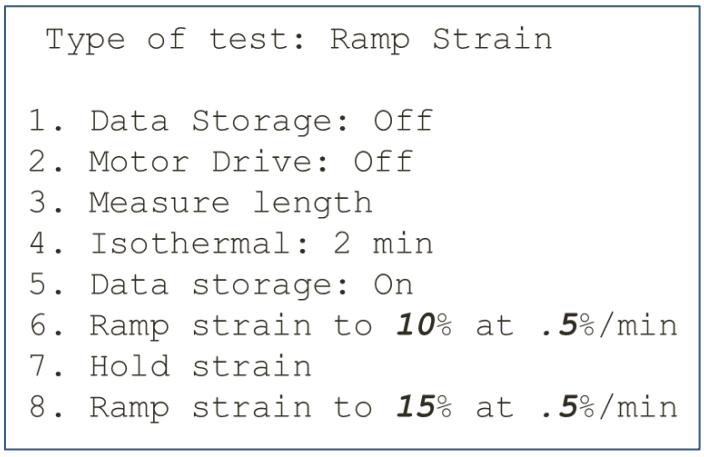

Figure 20. Itemized DMA procedure for the stress relaxation test performed for the LAPs. The light is turned on for a duration of 15 min, 2 min after the start of step 6.

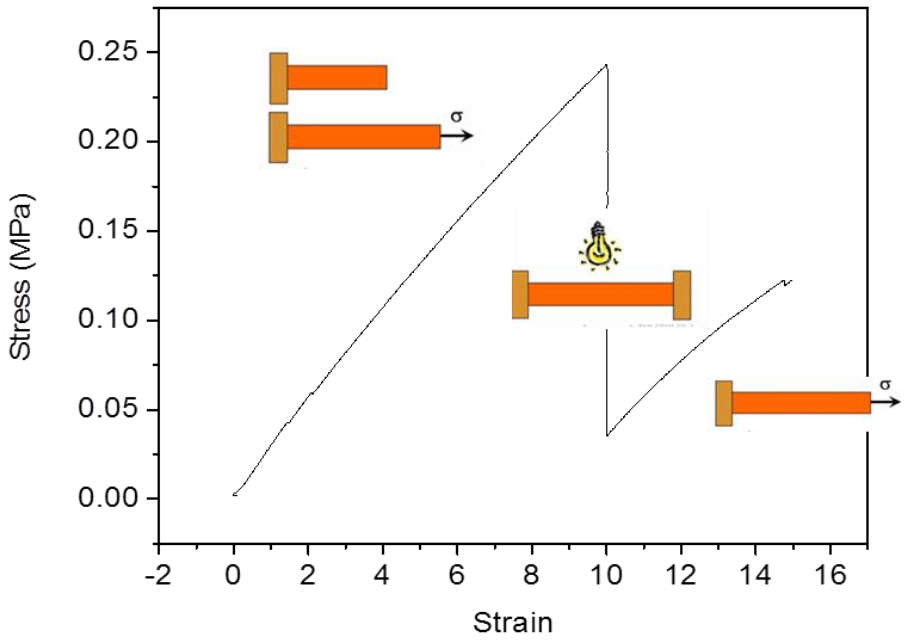

Figure 21. The expected stress-strain response of the LAP during the stress relaxation procedure

The potential of the LAP network to undergo network reformation and relax stress is dependent on the structure of the polymer network. The dependence of the stress relaxation on the crosslink density of the network was examined by performing stress relaxation tests on the three stoichiometric monomer ratios (2/5/3, 1/5/4, 0.5/5/4.5). Elastic modulus decreases, but chain mobility increases with the decrease in crosslink density. After preliminary analysis, the PETMP/MDTVE/EGDMP = 1/5/4 showed the best compromise between elastic modulus and crosslink density and was the composition of the copolymer used for the remainder of the experiments.

Intensity studies were also performed using the DMA stress relaxation setup. Since the activation of a photoinitiator is only dependent on the energy of the incident photons and not on the density of the photons hitting the surface, reflections onto the sample would prove to be a problem for

the patterning experiments. Since reducing the incident intensity would also reduce the reflections proportionally, the rate of stress relaxation response was measured as a function of applied intensity. These tests showed the most appropriate intensity for a 15 min irradiation step was 5 mW/cm^2, which was used for the remainder of the optically thin photopatterning experiments.

4.3 DMA Single Trench Photopatterning tests

Testing

Since the goal of this work is to create prescribed deformation, tests were done on this material to create distinct, localized regions of deformation by irradiating small portions of a 1D uniaxially strained material. The samples were placed in the DMA grips, and a mask was placed between the light source and the sample. A higher value of strain results in more deformation, so the maximum strain used for these experiments was 10%. For these tests, two types of masks were tested: transparency masks and borosilicate masks. Because of the inability of the transparency masks to both hold a rigid structure and be placed close enough to the grips to minimize the diffusion of light and increase the area of irradiation, borosilicate glass masks covered with electrical black tape were created to fit into the grips that provided a rigid structure close to the sample, with the added benefit that the glass would absorb any extraneous light at 365 nm. After the placement of the masks, the samples underwent the same testing procedure as the stress relaxation tests described above. After the DMA procedure finished, the samples were removed from the DMA grips and labeled and stored for measurement. The mask widths used were: 1 mm, 3.75 mm, 5.625 mm, and 7.5 mm.

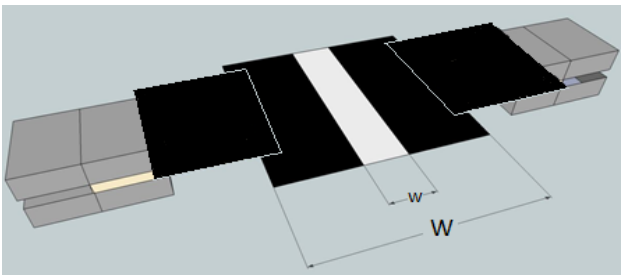

Figure 22. Schematic of the LAP sample placed in the DMA grips with a mask placed over the sample for the single trench patterning procedure

Measurement

The deformation of the sample caused by the network reformation was measured by coating the tested samples with deionized water and placing them onto borosilicate glass slides with a hydrophobic coating (Rain-X®). The water between the slide and the sample was removed using a Kimwipe; this process caused the length of the sample to adhere to the glass, including the regions of reduced thickness. This caused the profilometer to read twice the actual trench depth. A Dektak 6M stylus profilometer was used, with stylus tip of 1.2 micron diameter, a force of 3 microNewtons, and a resolution of .25 microns in the direction of the scan. These scans were taken as close to the middle as possible to eliminate any edge effects influencing the scans. Since the regions of reduced thickness adhered to the substrate, the measurements taken in the profilometer reflect twice the actual depth of the trench.

4.4 DMA Perioidic Photopatterning

Testing

After characterizing the effect of irradiating a single, localized region, multiple, periodic regions were irradiated in a similar manner. Similar to the single trench photopatterning tests, 10% strain was used to maximize the deformation obtained by the sample. Instead of placing a mask with a single

trench in between the light and the sample, a mask with multiple zones that would allow light through was placed in front of the sample. Cutting glass to create such a structure was not feasible for this application, so black masks made of an acrylate system were printed in an Objet Connex 260 3D printer to fit into the DMA grips, which provides both structure and appropriate distance from the sample. The periodic patterns studied were L/a = 0.25, 0.375, 0.5, and 0.75, where L was the length of a single irradiated zone and a was the period, which was 2mm for these tests. In each of these tests, masks with seven periodic regions were printed, resulting in a mask length of 14 mm.

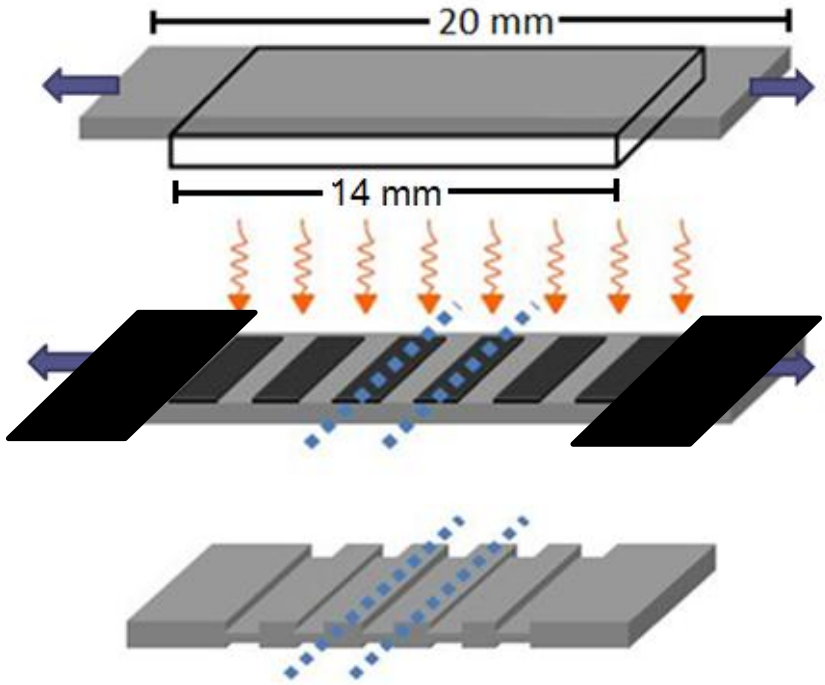

Figure 23. The LAP sample with a 20 mm gauge length is strained in the DMA, irradiated through a 3D printed mask, and released from the grips

Measurement

The deformation of the sample caused by the network reformation was again measured in the Dektak 6M profilometer. The sample was treated in a similar manner as with the single trench case and placed on a glass slide, again causing the profilometer to read twice the actual trench depth. Instead of taking a single scan across the length of each sample, the depth of each trench was measured individually, to provide enough flexibility to avoid inaccurate measurements caused by adherence of dust particles or air bubbles created during placement onto the slide. However, as with the single trench case the scans were taken as far from the ends (across the width) as possible to minimize the influence of edge effects. Scans were initially taken on both sides of the sample and confirmed symmetric behavior.

4.5 Stress Relaxation for an Optically Thick Sample

The optically thick sample was created with embedded UV photoabsorbers that absorb some of the photons with wavelengths in the UV to create attenuation of light through the thickness of the sample. However, the amount of added photoabsorber does not create a completely opaque sample, so given a dose of irradiation with a sufficient intensity and duration, enough photons can penetrate the sample to achieve the maximum amount of stress relaxation. These optically thick samples were tested in the same manner as the optically thin samples to compare and confirm that the maximum stress relaxation was still obtainable with the embedded UV photoabsorbers. These tests were done with both the Tinuvin 460 as well as the Tinuvin 5060. However, the Tinuvin 460 powder did not dissolve completely or evenly, so 3 wt% of the Tinuvin 5060 was used for the following optically thick tests.

4.6 Curving and Bending of Optically Thick Samples

The parameters used to control the deformation of the optically thick samples were: strain, light intensity, and time of irradiation. Since the deformation was the desired response, the residual stress did not to be monitored. As such, the following optically thick tests were performed in uniaxial grips with manual strain control.

Figure 24. Experimental set up with the mercury arc lamp and uniaxial strain tester in the UV hood used in the curving and bending experiments

Flood Irradiation

These optically thick samples were irradiated with different levels of intensity, duration, and applied strain. The deformation, not the stress, was the response to be monitored; therefore, the uniaxial tester was utilized to precisely control the strain and eliminate any drift that may occur in the DMA. Three distinct procedures were used to study the effects of intensity, duration, and applied strain on the resultant curvature. To measure the response of the intensity, the grips were placed 20 mm apart, and the samples were carefully placed in the grips, so that the sample did not have any slack. The gauge length, or the distance between the grips, was measured again with calipers. The measured value was then used to calculate the amount of elongation required for 10% strain. The sample was stretched to the desired length and then irradiated at values of intensity ranging from 5 mW/cm^2 to 40 mW/cm^2 in

increments of 5 mW/cm^2. To measure the response of the duration, the sample was placed in the grips in a similar manner. The sample was strained to 10% and the timer on the lamp was set to time durations in increments ranging from 30 sec to 90 min at an intensity of 40 mW/cm^2. The response of the applied strain was measured by placing the sample in the grips as before. The gauge length was measured to calculate values of strain ranging from 1%-22% (which was approximately the strain at break), and the sample was appropriately elongated. The samples were irradiated at 40 mW/cm^2 for a duration of 5 minutes. To measure the curvature of each test, the ~20 mm gauge length that was irradiated was cut out and then further cut into four 5 mm segments, to prevent the sample from curling up on itself and effecting the measurement of curvature. The samples were then placed on their sides and a photo of the samples was taken with a set of calipers to calibrate the image. A 3-point arc analysis was done using ImageJ software to calculate the curvature of the samples.

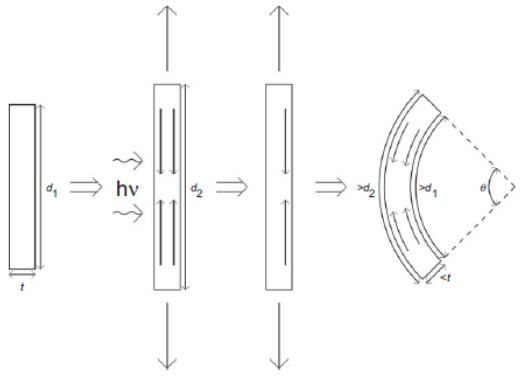

Figure 25. Curvature caused by the irradiation of an optically thick sample, (modified from [9]).

The strain vs. curvature produced the most results with the behavior that was most easily fit. It also had the best resolution and the highest degree of control. Therefore these results were later used as inputs for the ABAQUS model used by Dr. Xiaodong Cui to predict the deformation behavior of prescribed irradiated regions of varying width and strain.

Localized Irradiation

The deformation of localized regions of irradiation were tested and measured in the same manner as the optically thin experiments, with 20 mm x 4 mm x 0.152 mm sample irradiated at 40 mW/cm^2 for 5 minutes. However, since the evolution of stress was not a consideration for this set of experiments, the hinges were created in the uniaxial stage tester. By only irradiating a small region of the sample and inducing curvature on a small scale, hinge-like structures between non-irradiated zones were created upon release of the strain. For these tests, the hinge created was measured as a function of applied strain and irradiated width. A series of masks with different w/W ratios were created. These 100 ·w/W ratios were: 1, 2.5, 5, and 10. The values of applied strain were: 10%, 15%, 20%, 25%.

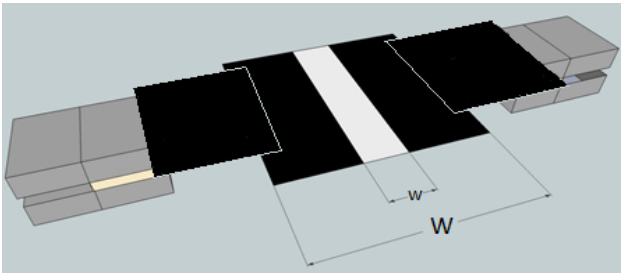

Figure 26. Setup for the optically thick hinge experiments, similar to the optically thin single trench photopatterning experiments

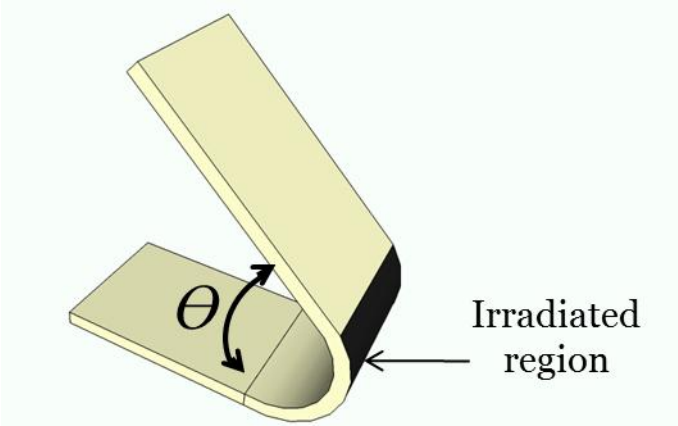

Figure 27. The predicted hinge created from irradiating a small, localized region of the optically thick sample

The angle created by these hinges was measured as a function of the applied strain and the width of the irradiated region. To remove the weight effect of the sample on the hinge angle, the samples were cut into 5 mm slices and set on their sides. Images were taken of the samples with a set of calipers to serve as a scale. The images were analyzed in ImageJ superimpose an angle onto the hinge to determine the interior angle created by the irradiation step. This step is depicted in Figure 28.

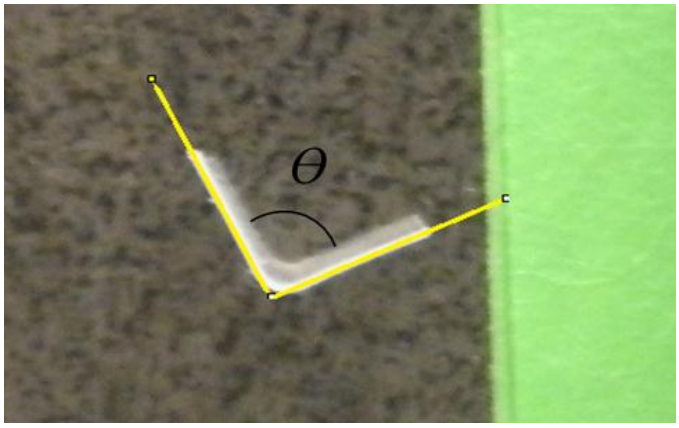

Figure 28. Image of the hinge imported to ImageJ with an angle superimposed onto the sample to measure the interior angle

4.7 3D Self-Assembling Structures

The parameter of strain was the most easily controlled, and had the highest degree of precision, so the linear fit for the curvature vs. strain curve data points was used as a basis to design the testing set up for structures that would “self-assemble” upon being cut out of the sample in an appropriate manner. The heart structure was created using a 30 mm x 4 mm x 0.152 mm sample as before and exposing it to two irradiation steps on opposite sides of the sample. The irradiation steps for the self-assembly for the heart were designed for a uniaxial sample 15.4 mm in length. However, to provide an appropriate gauge length for which the stress raisers do not influence the uniaxial stress state, a 20 mm gauge length between the grips was used. Upon release of the strain, the 20 mm of the sample was cut off to create a sample of length 15.4 mm that could fold into a heart. The first irradiation step was to strain the sample by 20% and then irradiate the sample through a 1 mm mask for 5 min at 40 mW/cm^2. The sample was then flipped over and the second irradiation step was to stretch the sample 5.5% and irradiate the sample through a mask with two open regions of length 4.8 mm.

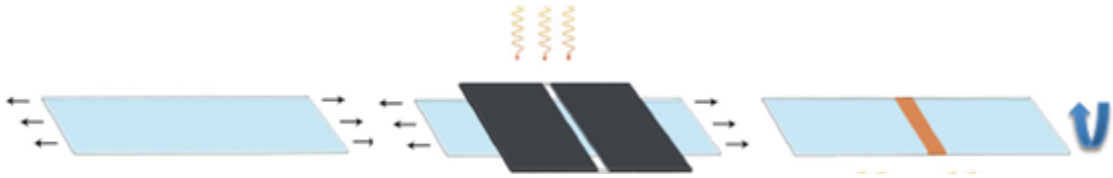

Figure 29. First irradiation step in creating the "self-assembling" heart
"

Figure 30. Second irradiation step in creating the "self-assembling" heart, on the flip side of the first irradiation

The resulting structure not only showed the ability to control the deformation on two length scales, but also that the material exhibited the ability for deformation on both sides of the sample. The second self-assembling structure demonstrated the homogeneity of the structure through the creation of two sets of hinges in perpendicular directions. This was also done through two irradiation steps. A 30 mm x 20 mm x 0.152 mm sheet was used. In the 30 mm direction, the sample was strained to 20% and irradiated through a mask with three 1 mm open regions. The sample was then released, and stretched in the perpendicular direction to a strain of 20% and irradiated through a mask with two 1 mm regions. The sample was then released from the grips, laid flat on a cutting board, and a cross was cut out in the shape shown in Figure 31, making sure to cut out the corners of the base to eliminate regions that obtained a double dose of irradiation.

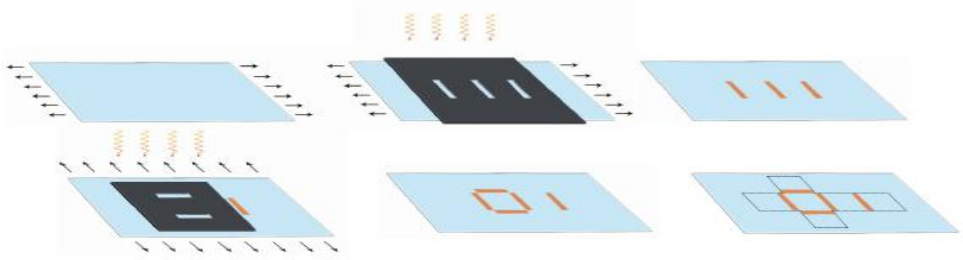

Figure 31. The two irradiation steps used to create the self-assembling cube structure. The sample was first strained in the x direction and irradiated through a mask with three irradiation zones. Then the sample was strained in the y direction and irradiated through a mask containing two irradiated zones that completed the four edges of the base of the cube. Upon release of the strain, the sample was then cut out along the lines shown above to allow it to curl up into a box.

5. Results

5.1 Optically Thin Flood Irradiation Stress Relaxation Results

Preliminary stress relaxation tests were performed to determine the appropriate stoichiometric ratio to use in the remainder of the LAP experiments. The effect altering the crosslink density was measured by monitoring the original elastic modulus, stress relaxation capability, and post-irradiation modulus for each of the three stoichiometric ratios of the monomers. Adjusting the crosslink density alters the elastic modulus according to the relationship:

$$E = 3\nu_E RT \tag{1}$$

where ν is the crosslink density [39], [40]. However, a decrease in the crosslink density also increases chain mobility, creating a higher potential for stress relaxation to occur. The elastic modulus of the samples was monitored because the network reformation caused by the RAFT reaction should not reduce the amount of crosslinks, but rather just alter how the network is connected. If the post-irradiation modulus is significantly different from the original modulus, then crosslinks are being cleaved, but not reformed, indicating that a mechanism other than the RAFT is causing a network change.

The requirements for a suitable sample are: a high enough elastic modulus to be handled easily, a large value of stress relaxation, and a small change between the elastic modulus of the original and reformed network. The following figures show the experimental data collected for the three monomer compositions for maximum strains of 3.5%, 4.5%, 6%, and 7.5%. The elastic modulus before and after the network reformation are noted.

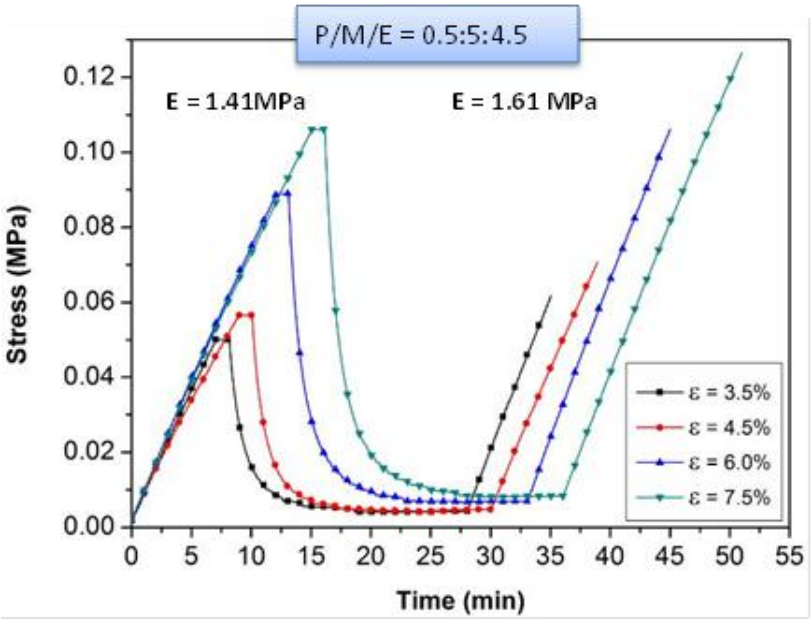

Figure 32. Stress relaxation test for the P/M/E = 0.5/5/4.5 composition with elastic modulus labed before and after the irradiation step

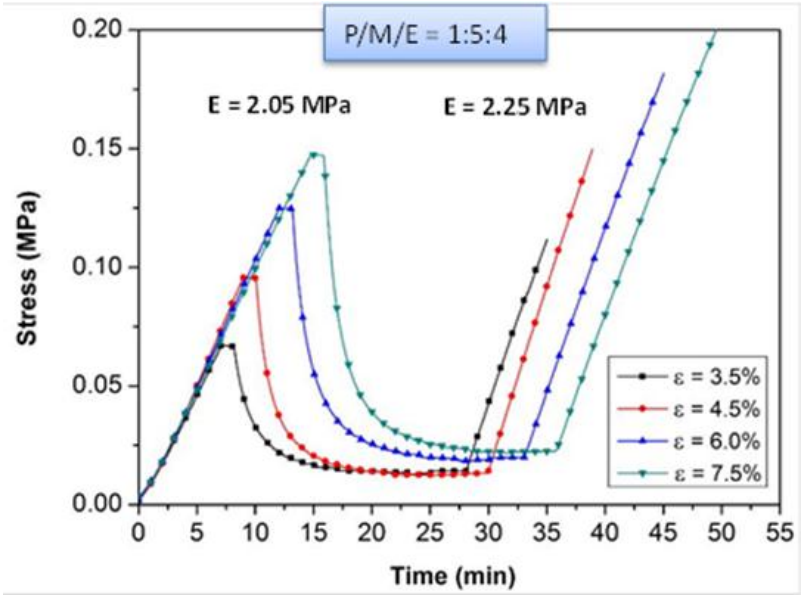

Figure 33. Stress relaxation test for the P/M/E = 1/5/4 with elastic modulus labeled before and after the irradiation step

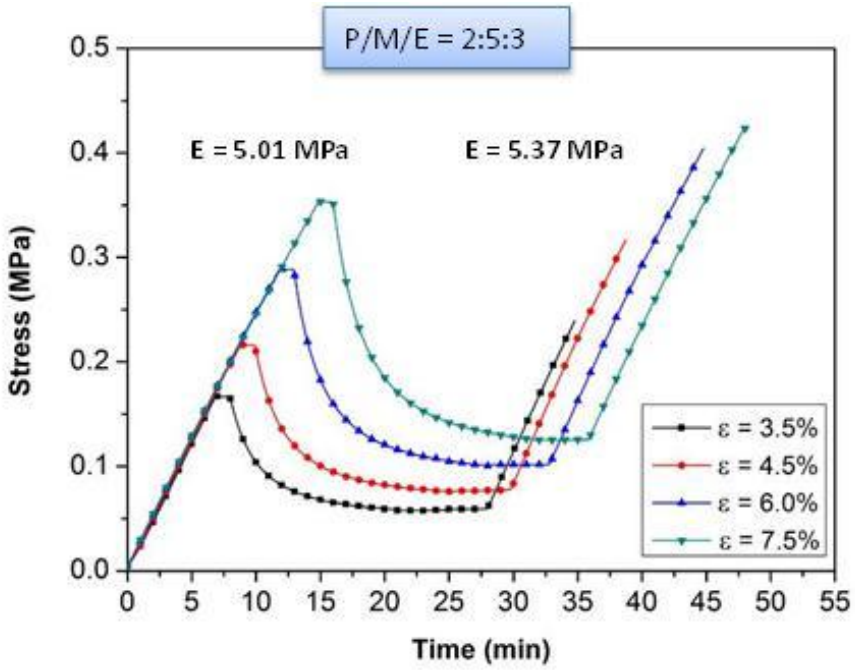

Figure 34. Stress relaxation test for the P/M/E = 2/5/4 with elastic modulus labeled before and after the irradiation step

Normalizing the stress measured in the DMA against the total stress applied to the system during the application of maximum strain results in the same amount of residual stress left in each system after the 15 minute irradiation step. This indicates that the stress relaxation percentage is independent of the strain applied and more clearly illustrates the effect of decreasing crosslink density on the maximum potential stress relaxation. The following curves show the normalized stress relaxation data for just the 15 minute irradiation step in the order of decreasing crosslinking density.

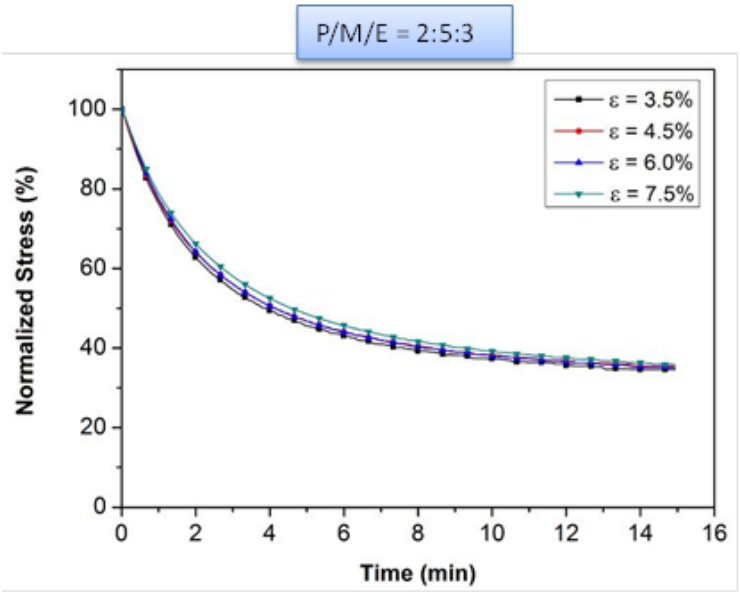

Figure 35. Normalized stress relaxation data for P/M/E = 2/5/3 for maximum strain values of: 3.5%, 4.5%, 6.0%, and 7.5%

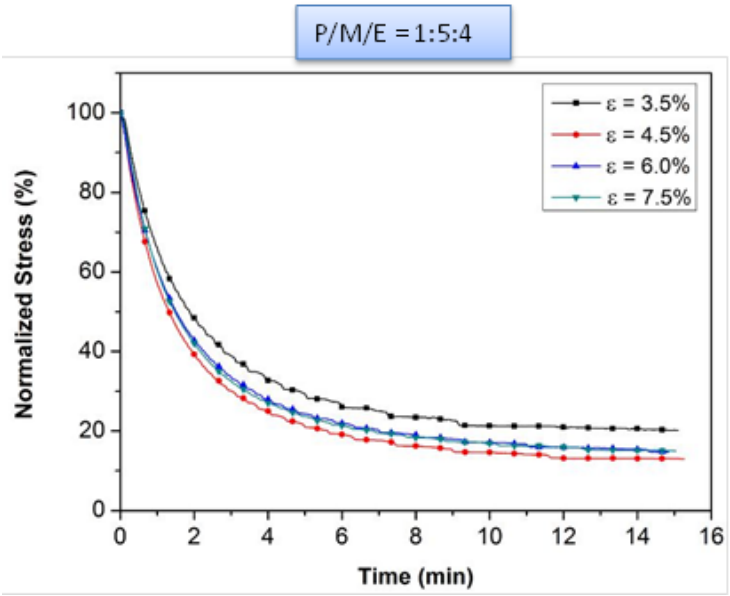

Figure 36. Normalized stress relaxation data for P/M/E = 1/5/4 for maximum strain values of: 3.5%, 4.5%, 6.0%, and 7.5%

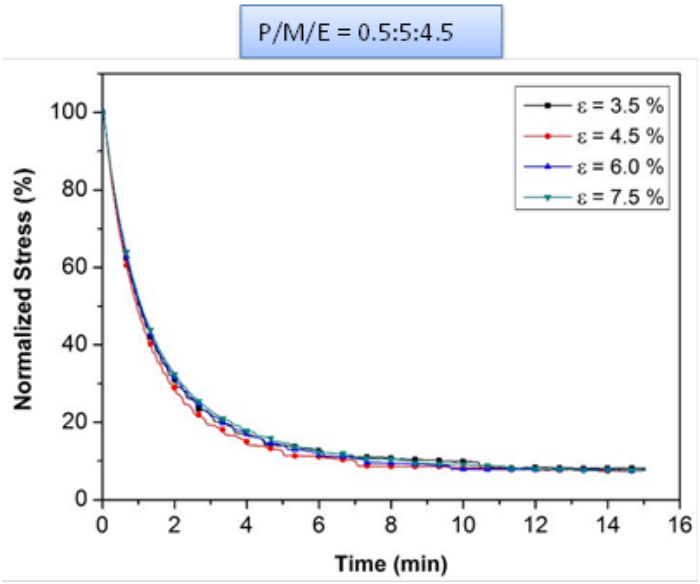

Figure 37. Normalized stress relaxation data for P/M/E = .5/5/4.5 for maximum strain values of: 3.5%, 4.5%, 6.0%, and 7.5%

The normalized data clearly shows the residual stress at the end of the irradiation step. This value was used to compute the amount of network stress relaxation for each composition, presented in Figure 38.

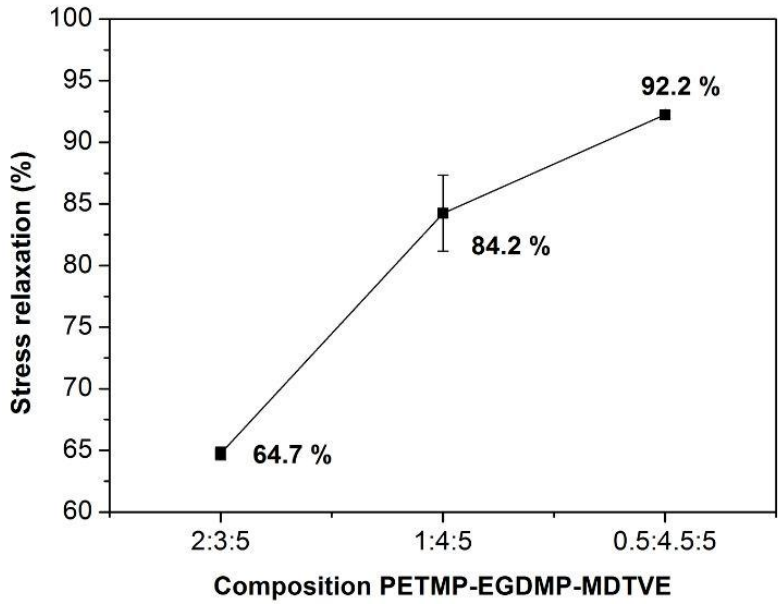

Figure 38. Stress relaxation obtained for the three compositions of the P/M/E LAP with the crosslinking density decreasing from left to right

Table 3. Summary of the Elastic Modulus before and after irradiation and amount of stress relaxed in the network

P/M/E Ratio	Original E (MPa)	Reformed E (MPa)	Stress Relaxation (%)
0.5/5/4.5	1.41	1.61	92.2
1/5/4	2.05	2.25	84.2
2/5/3	5.01	5.37	64.7

The results confirm the effect of the crosslink density on both the elastic modulus and potential for stress relaxation in the sample. However, the elastic modulus of ~1.5 obtained by the sample with the highest value of stress relaxation proved to be too elastic to work with easily. Therefore, the polymer network used in the subsequent experiments was the PETMP:MDTVE:EGDMP = 1:5:4 ratio due to the balance between the elastic modulus and stress relaxation potential. The subsequent finite element simulations were based on the total stress relaxation obtained by flood irradiating the sample. This was considered to be the maximum stress relaxation obtainable by the sample.

For the flood irradiated stress relaxation tests, finding the maximum potential for the stress relaxation obtainable was the objective. As such, a high intensity was used and reflections from the grips were not a concern. However, this was a concern for the design of the photopatterning experiments because reflections hitting the back of the sample in the regions that were meant to remain unreformed diminishes the effect of the surface patterning. As such, tests were performed to examine the effect of reflections from the testing setup. In spite of the precautions taken when constructing the setup with light absorbing paper, there was some measurable intensity hitting the back of the sample, on the order of hundreds of microWatts/cm^2. A stress relaxation test was performed using the same set up at the lowest level of intensity for the lamp. The intensity of the incident irradiation describes how many (how dense?) photons are hitting the sample; the wavelength dictates the energy of the individual photons.

Since the homolytic cleavage is only dictated by the energy of the photon, network reformation will occur at any intensity of UV light with the appropriate wavelength. The following plot demonstrates that given the time scale for the stress relaxation test, 10% of the irradiation intensity can cause almost 40% of the maximum potential stress relaxation during the 15 min irradiation step.

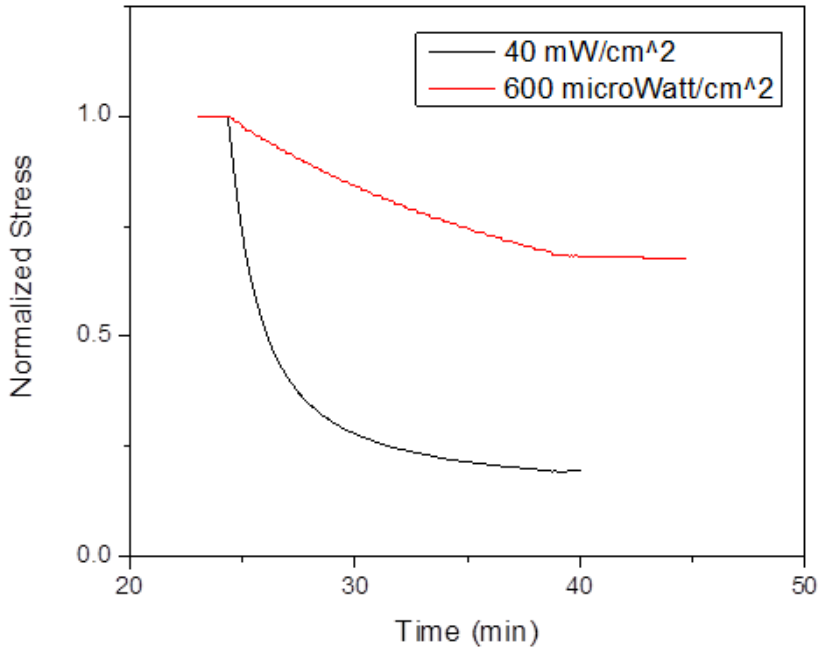

Figure 39. Comparison of the stress relaxation obtained using the lowest setting on the Omnicure mercury arc lamp with the intensity used for the initial flood irradiation tests.

Because of the magnitude of the impact of slight reflections, designing an appropriate experiment was a compromise between reducing extraneous sources of irradiation and minimizing the duration of the test. Sufficient time was required for the sample to realize the maximum potential of stress relaxation, which was dependent on the rate of rearrangement. However, each test at 40 mW/cm^2 took over an hour, which dictated the need for the minimization of irradiation time. The rate at which the network reformation occurs is dependent on the rate the photons break the C-C double bond

in the allyl sulfide functional group which is controlled through the intensity of irradiation. Previous work has been done to demonstrate how the intensity of irradiation affects the rate of stress relaxation [9]. However, this was done with a different system, so the effect of the intensity on the rate of stress relaxation for the current LAP system was performed using the same testing method and setup as the stress relaxation tests for varying doses of irradiation: 5 mW/cm^2, 10 mW/cm^2, 25 mW/cm^2, and 40 mW/cm^2. The stress relaxation curves were fitted with an exponential decay fit in Origin Pro 8, and the time constants for each case were compared. Irradiation at 5 mW/cm^2 was the limit for which the material was sufficiently relaxed during the irradiation time of 15 minutes and therefore induced the least amount of reflections on the back of the sample.

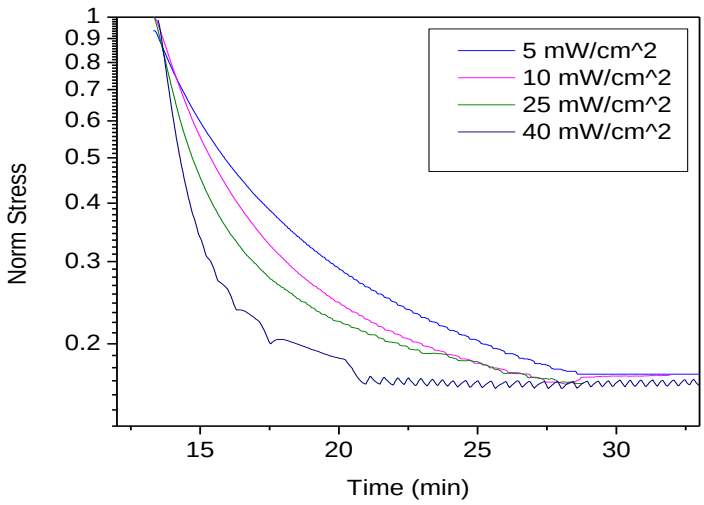

Figure 40. Experimental study on the effect of light intensity on the stress relaxation rate for varying levels of intensity for the current LAP system.

The following table presents the value of the characteristic time constant obtained for the varying levels of intensity.

Table 4. Measured time constants for fitted exponential decay curves for varying doses of irradiation

Intensity (mW/cm^2)	Time Constant (min)
5	3.45
10	2.43
25	1.76
40	1.03

As expected, the time constant decreases with an increase in the density of photons hitting the surface of the sample. The relationship is approximately linear with decreasing time constant as the intensity increases and is presented in Figure 41.

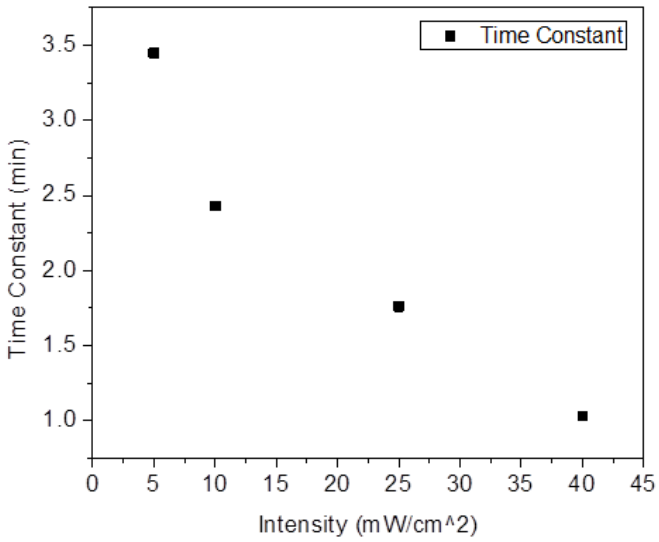

Figure 41. Graphical representation of the time constants fitted from exponential decay curves as a function of the intensity of irradiation (mW/cm^2)

5.2 Comparison of the Polymer Network with Rubbery Elasticity Theory

Equation 1 provided above describes the rubber elasticity theory. This equation was used to compare the experimentally obtained elastic modulus with the theoretical modulus of the provided system. The value of the theoretical crosslink density was calculated by assuming that the vinyl ether underwent polymerization with the thiol groups indiscriminantly, such that the thiol groups from the PETMP were indistinguishable from those from the EGDMP. Given the P:M:E = 1:5:4 eventually chosen for the remainder of the experiments as a result of the balance between the elastic modulus and maximum stress relaxation potential, the ratio between the tetra functional monomer and the linear monomer is 1:4. This results in a vinyl ether group polymerizing with a thiol group from the crosslinker one third (1/3) of the time, which provides a crosslink density of 0.33. The corresponding elastic modulus is 0.24 MPa. This value was compared to the stress-strain results obtained from the DMA during the stress relaxation test provided in Figure 42.

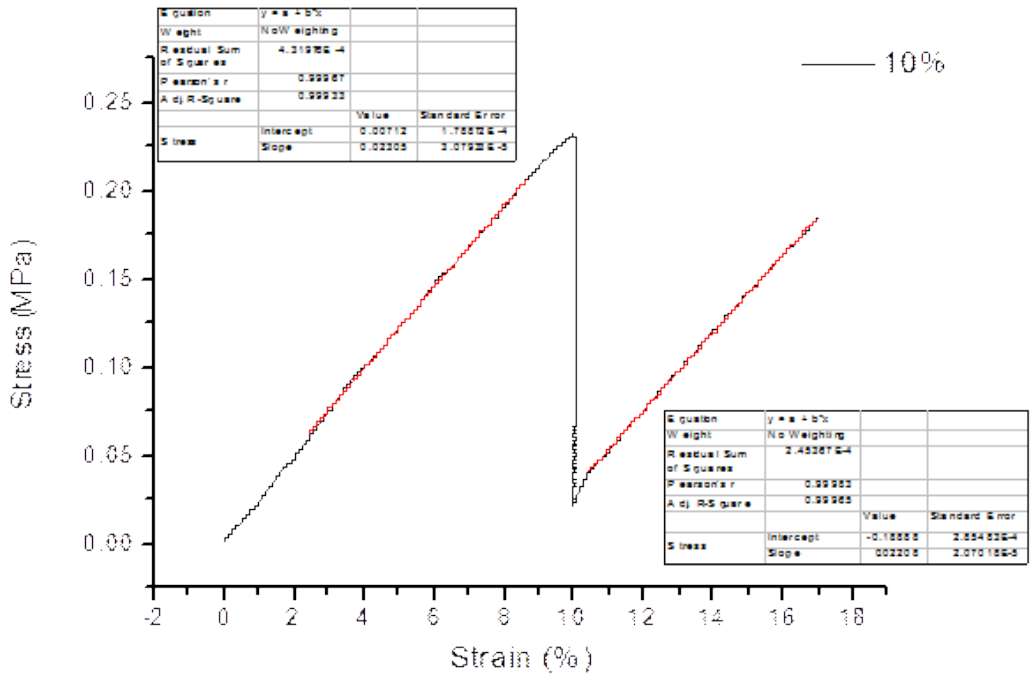

Figure 42. Stress-strain curve obtained from the DMA during the stress relaxation procedure with a maximum strain of 10%

The value of the experimentally obtained elastic modulus was 2.3 MPa, both before and after the polymerization step. This is with 5% of the theoretical value, confirming that the network approaches the theoretical network and the consistent modulus before and after the network reformation step supports the assumption that for each bod that is broken, another one is formed, conserving the crosslink density in the material.

5.2 Single Trench Photopatterning Results

The two parameters compared for the single trench tests were the amount of residual stress left in the system and the depth of the trench created by the stress relaxation. The DMA allowed real time measurement of the stress during the irradiation step, and the depth of the trench was measured in the Dektak 6M profilometer. Since only a localized region of the gauge length was irradiated, the final deformation was a balance between the irradiated region that contains the reformed network with a "stress-free" configuration and the unirradiated region. During the irradiation step, the irradiated region continuously tries to relax the stress in the material, which creates a larger trench depth for the small irradiated areas.

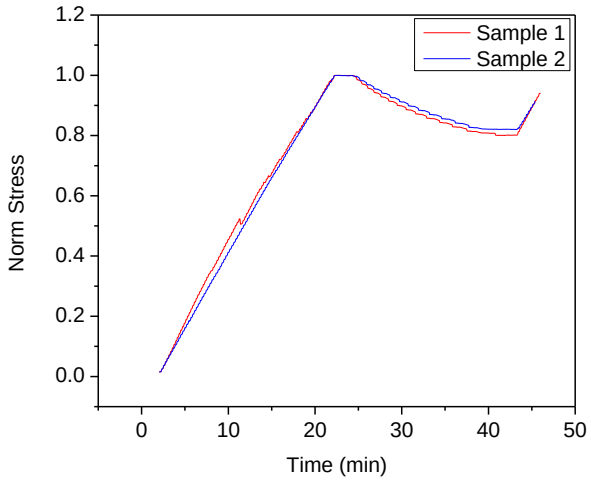

Figure 43. Stress relaxation results for irradiation of the sample through a 1 mm mask

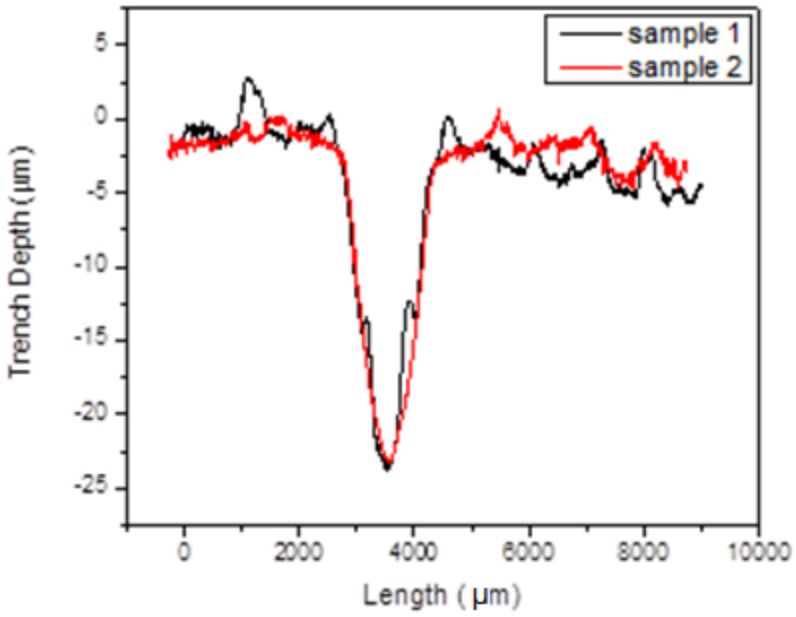

Figure 44. Graphical representation of the surface feature created through irradiation through the 1mm mask

In order to ensure that only the desired region was being irradiated, the sample was irradiated through the material used to cover the "dark" regions of the sample. In this test, the same stress

relaxation procedure was used, which resulted in the sample being held at the maximum strain of 10% for a total of 30 minutes. During this time, the material relaxed ~2% of the stress. However, due to the low intensity tests, this reduction of stress may be just an effect of the viscoelasticity of the material. The experimental results compared the same stress relaxation procedure without a mask is presented in

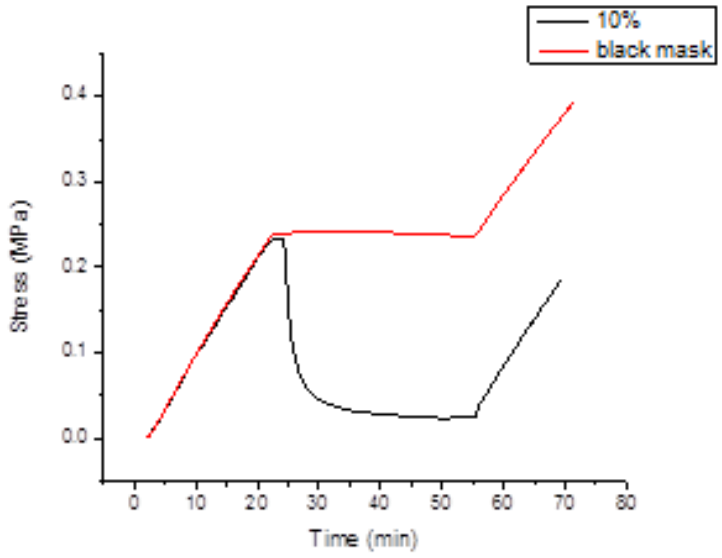

Figure 45. Comparison of the flood irradiated stress relaxation test with a maximum strain of 10% with the same test done with a completely opaque borosilicate mask placed in front of the sample

The simulation uses the flood irradiation stress relaxation results to define the volume fraction undergoing network reformation during the irradiation procedure. The finite element analysis was done by Xiaodong Cui in ABAQUS using 3D solid elements with 20,000 elements in total. For the best resolution, the irradiated region was more densely meshed to capture the deformation within that region. The model works under the assumption that the unirradiated region completely recovers all of the applied strain and undergoes no deformation. The experimental procedure mimicked the simulated procedure well enough that there was good agreement between the experimental data and the simulated results. The following compares experiment to the simulation for the two measurements of

interest throughout these procedures: the stress relaxation obtained through irradiation of a small region and the subsequent deformation.

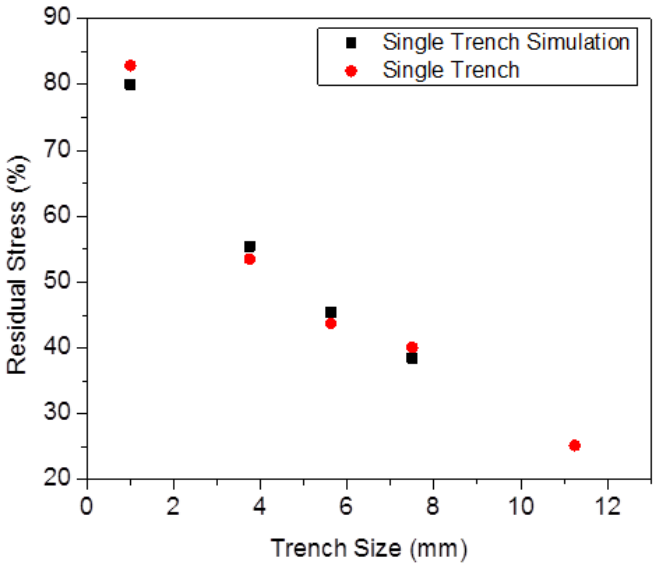

Figure 46. Comparison of the stress relaxation observed experiments with the FEA simulation for irradiating a single, localized region

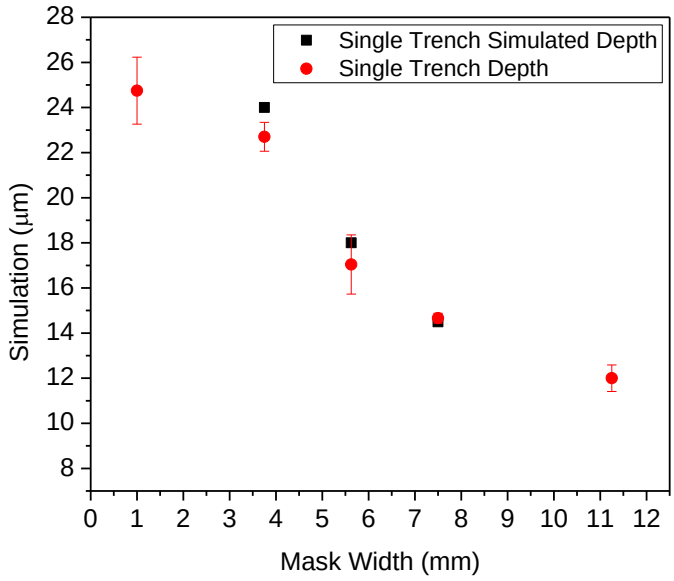

Figure 47. Comparison between the experiments and the simulation for the trench depth that results from irradiating a single, localized region

The data presented in Figure 47 is the measure of the maximum deflection measured in the Dektak 6M profilometer. As a result, it is a comparison of twice the trench depth, according to the procedure presented previously.

5.3 Periodic Trench Photopatterning Results

In this set of experiments, multiple, distinct regions were irradiated as described in the procedure. Each individual trench in a sample was scanned separately to provide ease in the aligning the sample to get the cleanest results. Taking the scans separately also allowed better comparison of the individual trench depths after the scans; drift in the profilometer caused a slight slope in the data and created the need for alignment of the data during post-processing. Figure 48 shows a comparison

between scans taken for individual trenches from a sample irradiated through an L/a = 0.25 mask. These samples were more subject to touching the 3D printed mask during the experimental setup, causing particles of dust to adhere to the sample. Therefore, these samples have much more noisy scan, further requiring the need for individual scans for the individual trenches. The following scans compare the trenches within a single sample for the four mask sizes. As the L/a ratio increases, it is clear that the sample has bottomed out onto the slide because of the flat trough becomes more evident. During the surface profilometry, some trenches had collected enough dirt or had ripped and data could not be obtained from these regions.

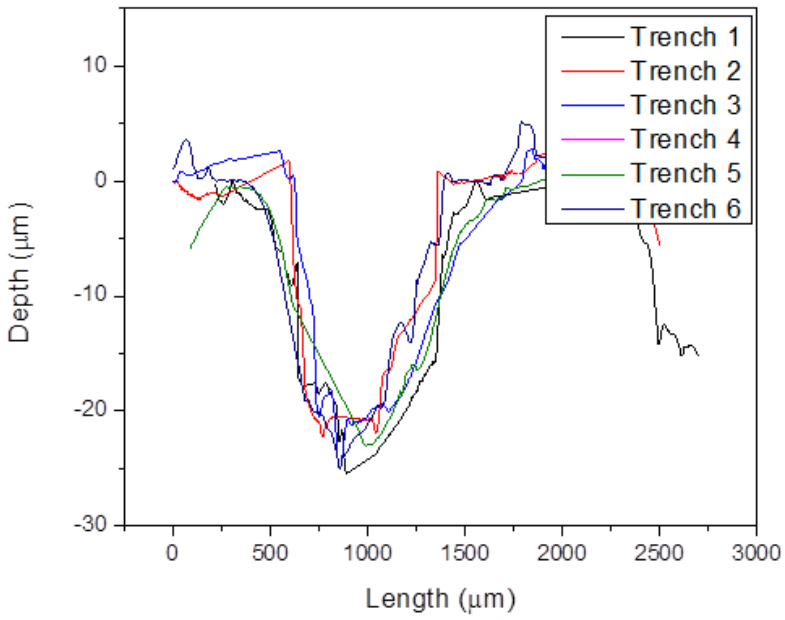

Figure 48. Trench depths as a function of length obtained from the same sample plotted on top of each other for the L/a = 0.25 sample

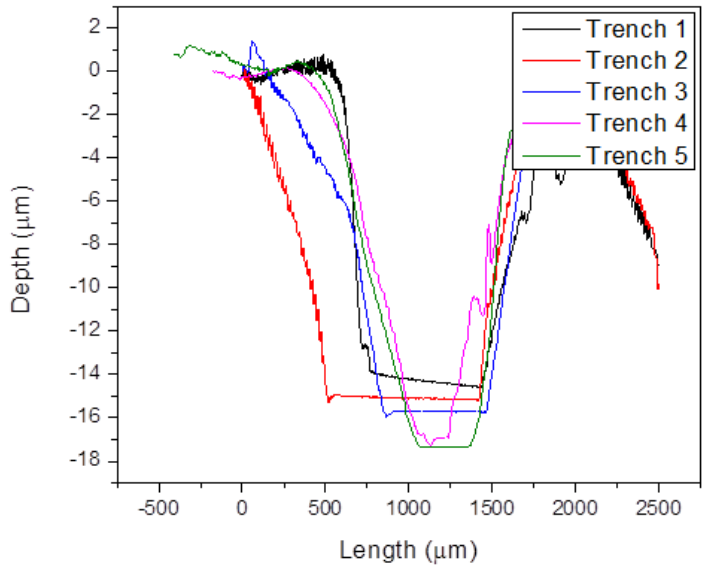

Figure 49. Trench depth as a function of scan length obtained from a single sample irradiated through an L/a = 0.375 mask

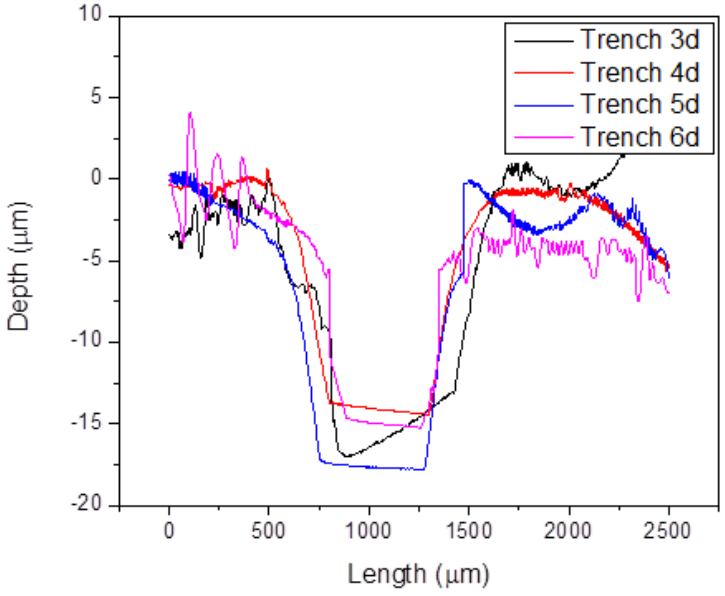

Figure 50. Trench depth obtained from the surface profilometer as a function of scan length obtained from a single sample irradiated through a physical mask with L/a = 0.5

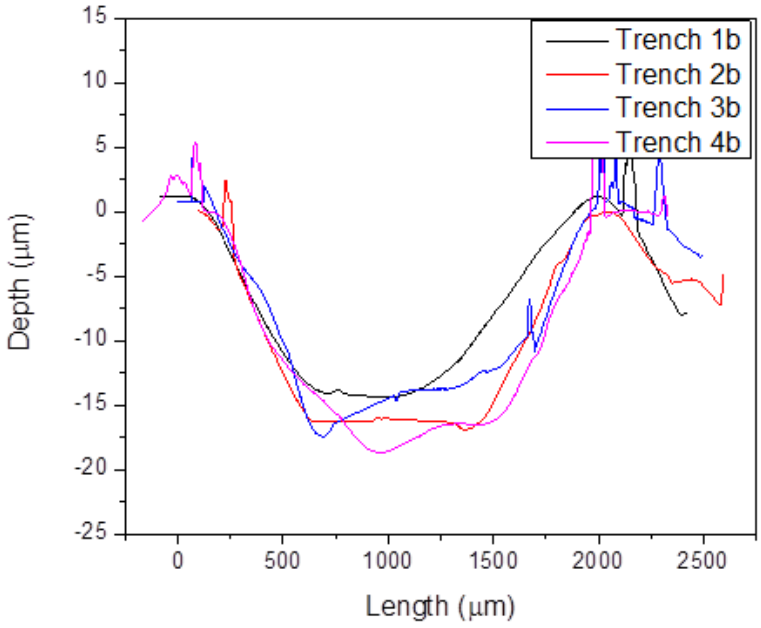

Figure 51. Trench depth measured in the surface profilometer as a function of scan length obtained from a single sample irradiated through a physical mask with L/a = 0.75

The following plot shows the full length scan of a sample irradiated through an L/a = 0.25 mask. The depths given by the difference between the top and the bottom of the trenches is approximately uniform. However, there seems to be a slightly parabolic trend in the depths. This is probably a result of the poor collimation and a slight deviation in the alignment of the light guide. This would create a slightly higher intensity in the middle of the spot size, providing a different stress relaxation response.

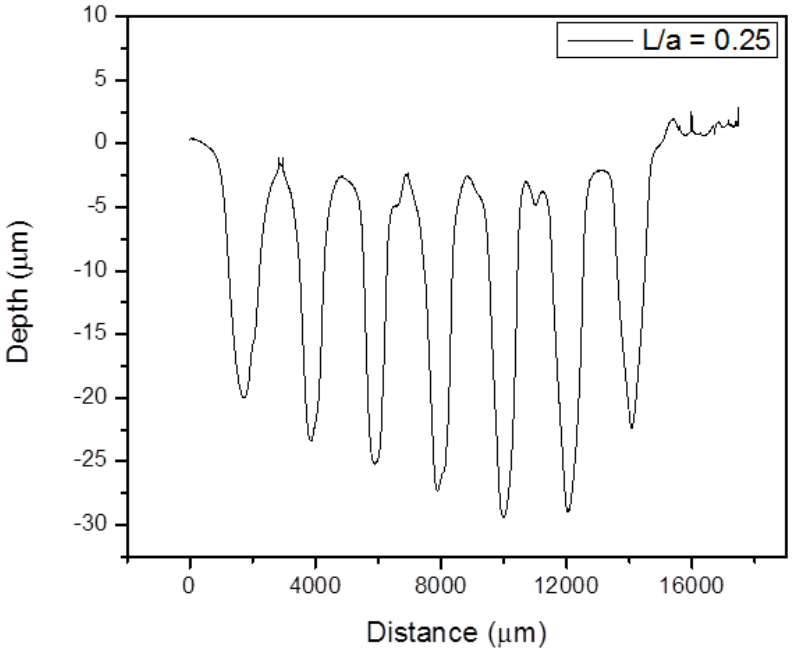

Figure 52. Surface profilometer scan of the entire length of a sample irradiated through a mask ratio L/a = 0.25

With these tests, the stress and the trench depths were measured and compared to the ABAQUS simulation. The results are presented as a function of the mask ratio L/a.

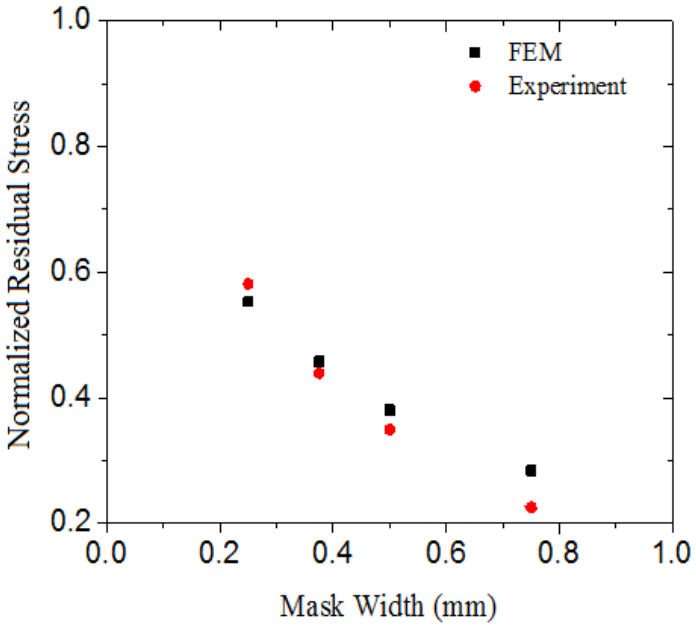

Figure 53. Comparison of the FEM results and the experimental result for the stress relaxation obtained from different periodic masks as a function of the effective irradiated area

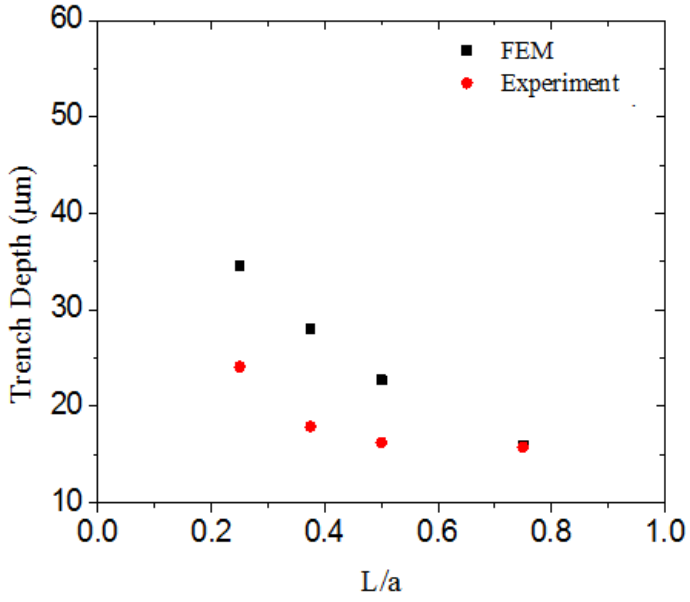

Figure 54. Plot comparing the FEM results for the predicted trench depth and the measured trench depths as a function of the mask ratio

The comparison of the experimental results to the FEM for the periodic trenches shows a significant disparity, except for the L/a = 0.75 case. The two cases seem to follow two distinct trends. This indicates that the behavior of the material is not fully understood.

5.4 Comparison of the Simulation Results as Function of Irradiated Area

The difference between the single trench and periodic response was evaluated to determine the effect of periodicity on the overall result. The responses were compared as a function of effective irradiated length. This was computed for the periodic case by multiplying seven times the L value.

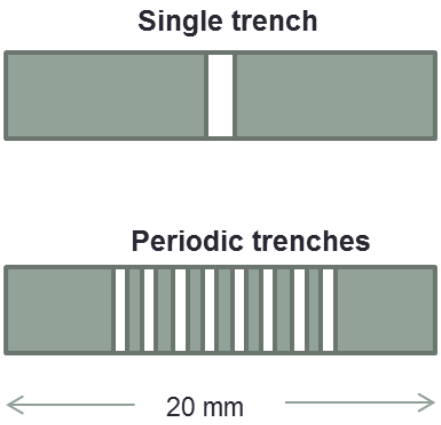

Figure 55. Comparison of the two photopatterning cases

Table 5. Conversion of periodic L/a ratio to effective irradiated length for comparison with single trench tests

L/a	Effective Irradiated length
0.25	3.5
0.375	5.25

0.5	7.0
0.75	10.5

The first parameter compared was the residual stress left in the system. The responses for the single trench and periodic cases seem to follow a similar trend, which indicates that the stress relaxation response is primarily dependent on the area of irradiation.

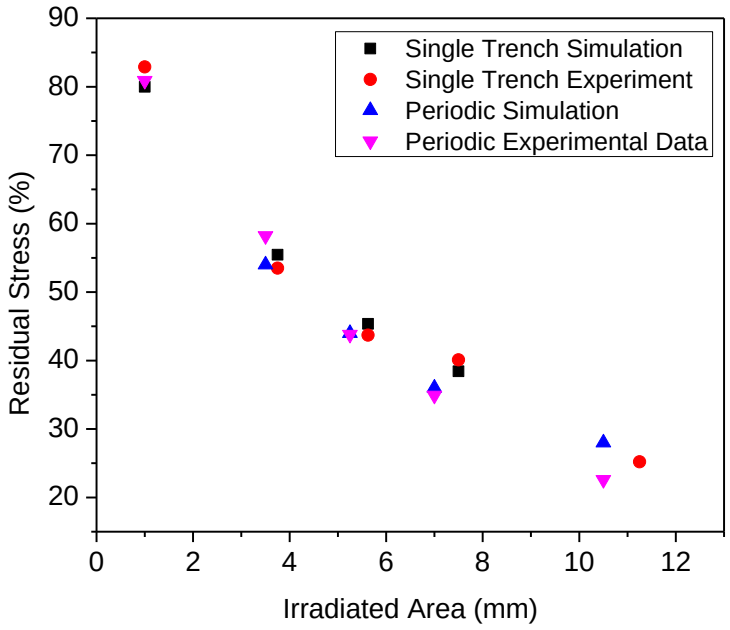

Figure 56. Residual stress left in the system after irradiation through single and periodic photomasks plotted as a function of irradiated length

Additionally, the simulation results for the trench depths of the two cases were compared as a function of irradiated area. These two data sets seem to follow two distinct trends, despite the similarity in their stress relaxation response.

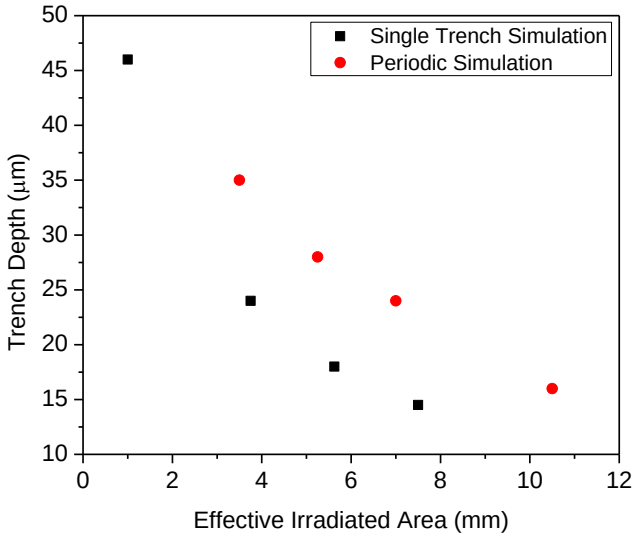

Figure 57. Comparison of the trench depths predicted by the FEM for the single trench and periodic cases

Because the periodic data did not fit the prediction form the simulation very well, the periodic trench depths were compared to those predicted by the single trench FEM simulation. While there simulation had not been performed for the same irradiated areas, the following plot shows the comparison of the experiment to values close to the same irradiated area. While there is a distinct difference at the smallest mask width, the trend shows a much better correlation than the periodic simulation, suggesting that the area is the most influential component of the experimental setup.

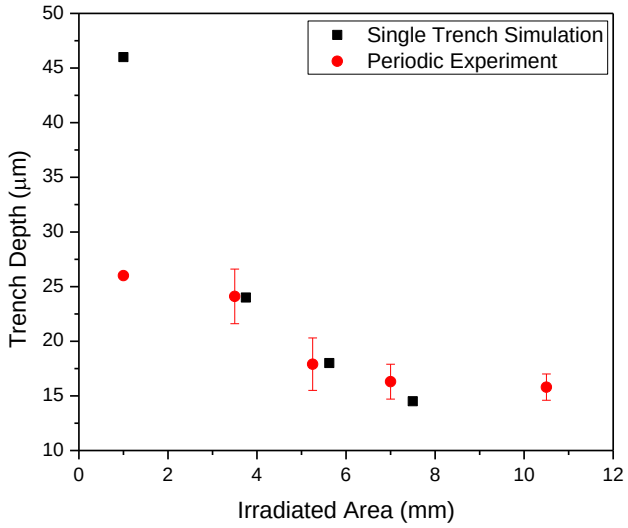

Figure 58. Comparison of the trench depths for the single trench simulation to the periodic experiment

The following compares the trench depth values found from both experiments to the trench depths obtained from the single trench FEM analysis, to summarize the results found in the patterning tests. This indicates that the understanding of the system is sufficient to predict the amount of network reformation and surface deformation created by irradiation through a single photomask, but not to predict the behavior of multiple irradiated areas.

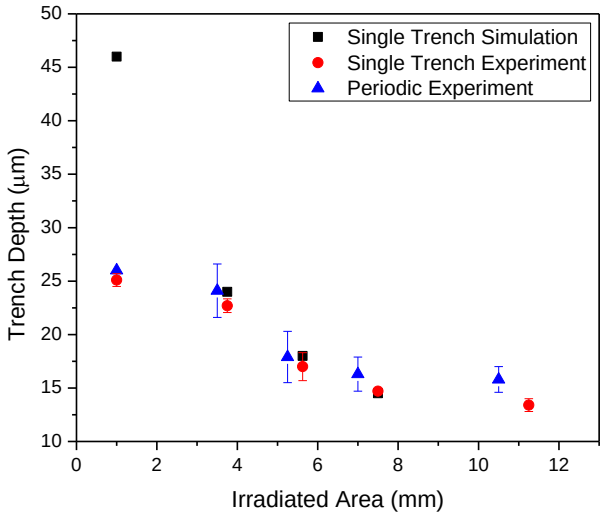

Figure 59. Comparison of the trench depths obtained from both experiments with the trench depths obtained from the single trench FEM simulation

5.5 Optically Thick Stress Relaxation Results

In order to create effective "optically thick" samples, samples were created that were relatively optically thin in the visible range (400-500nm) to ensure complete polymerization of the sample, but create attenuation of light within the UV regime around 365nm. To do this, UV photoabsorbers were added with absorbance spectra that peaked in the 365nm range, but dropped off at wavelengths longer than 400nm. To confirm that the material was optically thin in the visible range and optically thick in the UV, a UV-Visible absorption spectrometer was used to measure the transmittance of the sample at varying wavelengths. With this, the transmittance values were scanned for a range of wavelengths at 10mW/cm^2. For the samples with and without the photoabsorbers, there was little to no attenuation of the visible regime, with a transmittance value around 97%, indicating that the polymerization process will occur homogeneously through the thickness for all the samples. At wavelengths shorter than 400 nm, the sample without any added photoabsorber is reasonably optically thin with a transmittance

value around 75%. However, there was a distinct drop off in the transmittance for the samples with embedded photoabsorbers.

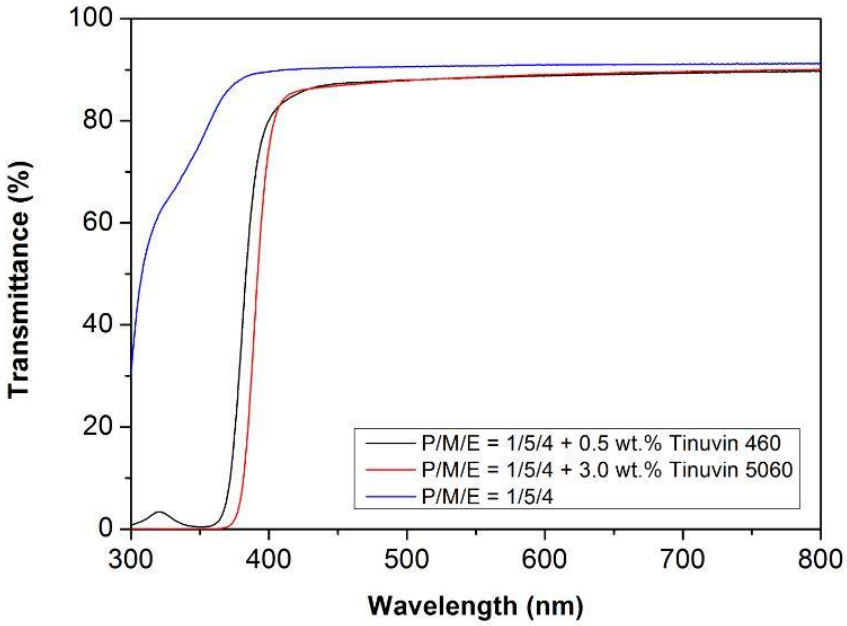

This confirms that the sample sufficiently attenuates light at 365 nm. Two factors of the photoabsorbers resulted in the use of Tinuvin 5060 in the experiments. First, the transmittance drops off at a shorter wavelength for the Tinuvin 460. Therefore, Tinuvin 5060 creates more attenuation at 365 nm. Also, Tinuvin 460 is a powder and Tinuvin 5060 is a viscous liquid. It was difficult to completely dissolve Tinuvin 460 into the sample before ambient light and the heat of mixing caused the monomer solution to start polymerizing and become too viscous to inject between two glass slides offset by 152 microns.

Stress relaxation tests were performed for the optically thick samples similarly to the optically thin samples. The samples are not completely opaque, and there is a finite quantity of photoabsorber. Therefore, the material should be able to reform the same volume fraction as the optically thin case, given a high enough intensity for a sufficient amount of time. Therefore, the added photoabsorbers

should affect the stress relaxation rate, but not the potential of the system to undergo network reformation. Controlling the amount of photoabsorber adjusts the amount of attenuation through the thickness of the sample. A steep gradient was desired for the sample, therefore 3 wt% of the UV photoabsorber Tinuvin 5060 was embedded into the existing LAP system. The following DMA results show that the sample still obtains ~84% stress relaxation during the irradiation step. However, instead of almost all of the network rearrangement occurring in the first few minutes, close to the entire 15 minutes of the irradiation step is required to reach the maximum value of stress relaxation.

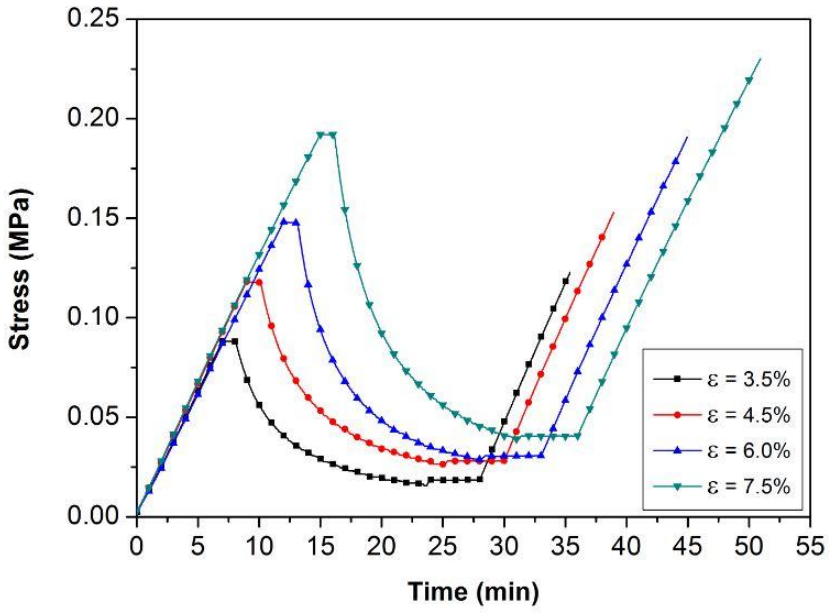

Figure 60. DMA results for the stres relaxation test performed on the optically thick samples

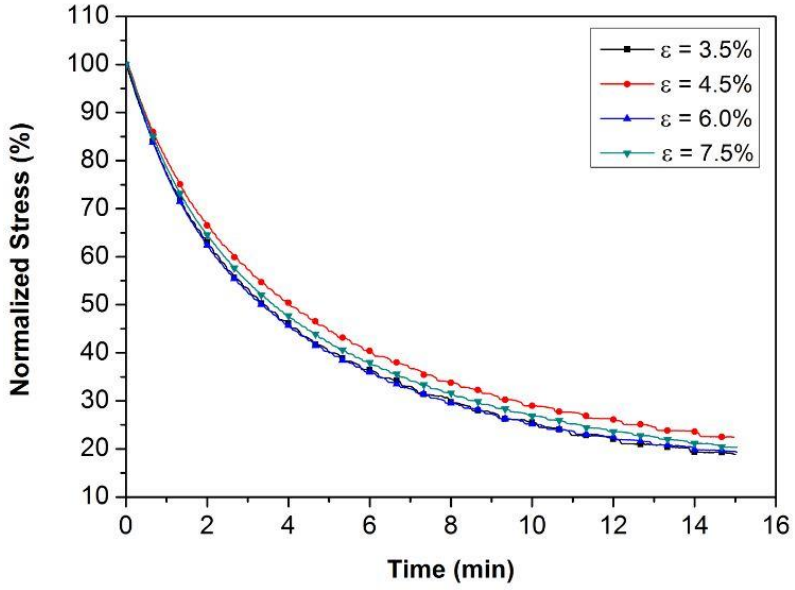

Figure 61. Normalized stress relaxation response for the optically thick samples (data shown for only the irradiation step)

The stress relaxation procedure for the optically thick samples was identical to the stress relaxation tests for the optically thin specimens. Due to the UV photoabsorbers, some of the photons emitted do not initiate the cleavage of the photoinitiator to create radicals. Therefore, the rate of the network reformation response is significantly slower than for the optically thin test at the same irradiation intensity.

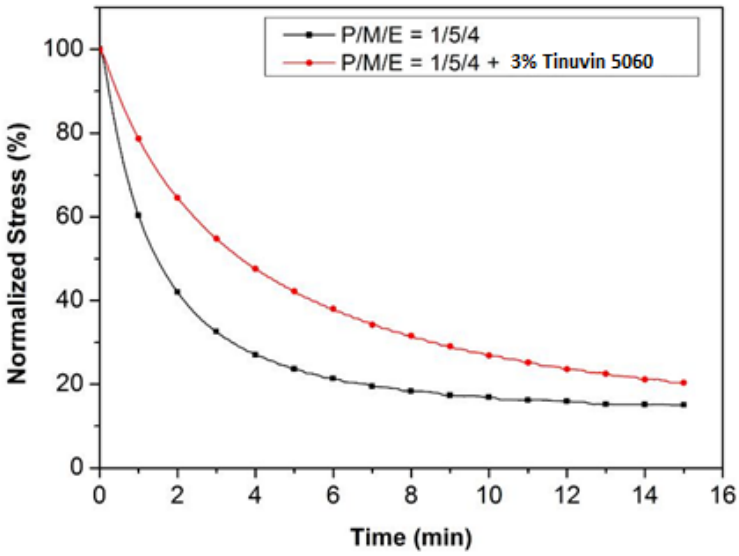

Figure 62. Comparison of the stress relaxation rate between the optically thin and optically thick samples

5.6 Curvature Results

The UV photoabsorbers embedded in the system create a gradient of light penetration through the sample at any given time and induce a gradient in the rate at which stress relaxation occurs at different levels of thickness in the sample. Varying values of residual stress in the material cause non-uniform deformation through the thickness, which induces bending of the material. The larger the difference in the stress states, the higher the induced curvature upon release of the strain. To control the amount of curvature created by flood irradiating the sample, the parameters of light intensity, duration of irradiation, and applied strain were adjusted. The intensity of the light and the duration of the irradiation dose were adjusted to control the amount of photons penetrating the sample, and adjusting the applied strain dictated the deformation of the reformed network. Previous work has been done to model the curvature dependence on these parameters based on a given absorptivity and thickness. However, the MSDS for the UV photoabsorber Tinuvin 5060 was unavailable, so only the trends could be compared, as opposed to values of curvature.

By controlling the applied strain in the experiment, the length of the reformed network can be adjusted. The difference between this deformed length and the undeformed length controls the subsequent curvature of the material. To investigate the effect of applied strain on the subsequent curvature, the sample was elongated to varying values of strain and irradiated at 40 mW/cm^2 for 5 minutes using the timer on the lamp. The following figure shows the average value of curvature taken from the experimental data, with error bars indicating the standard deviation of the four segments taken from the sample, as well as the fitted curve used in the ABAQUS simulation. The images used to measure the curvature are also compared to the results from the simulation, as a function of the applied strain.

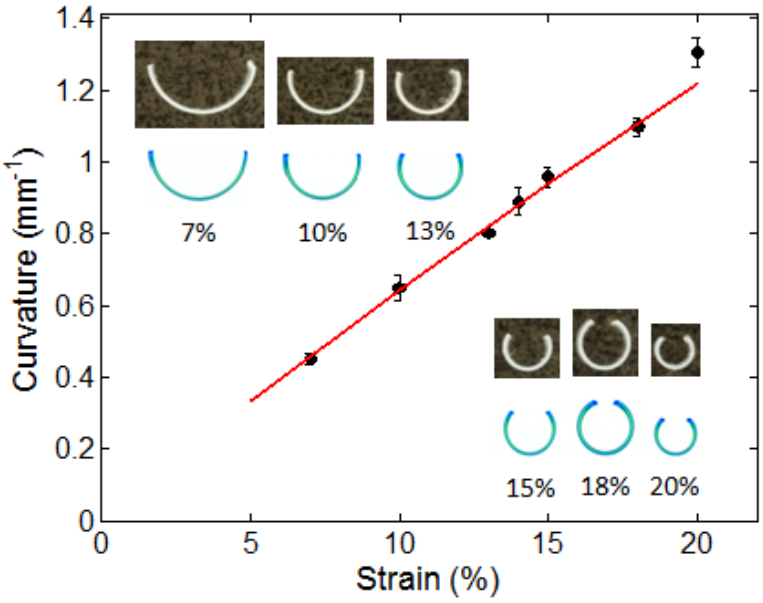

Figure 63. Curvature resulting from irradiation of the optically thick sample for 5 min at 40 mW/cm^2 for different values of strain. The red line indicates the fitted curve used in the ABAQUS model, and the results of the simulation are compared to the images obtained from the experiment [41].

Time was also used as a method of controlling the curvature induced in the sample. Instead of controlling the deformation of just the reformed network, the depth of the irradiation was controlled by

altering the length of irradiation. The longer the sample was irradiated, the more photons were able to initiate radical formation and the deeper into the sample the photons could penetrate. The effect of increased radical formation initially increased the curvature by increasing the amount of stress relaxed in a small fraction of the thickness at the top of the sample. Beyond a critical length of time, the depth of light penetration dominates and causes a decrease in the radius of curvature. However, even with a sufficiently long irradiation time, the curvature does not return to zero, supporting the postulation that the initiator can diffuse through the network and the gradient of stress relaxation through the thickness of the material will always be present.

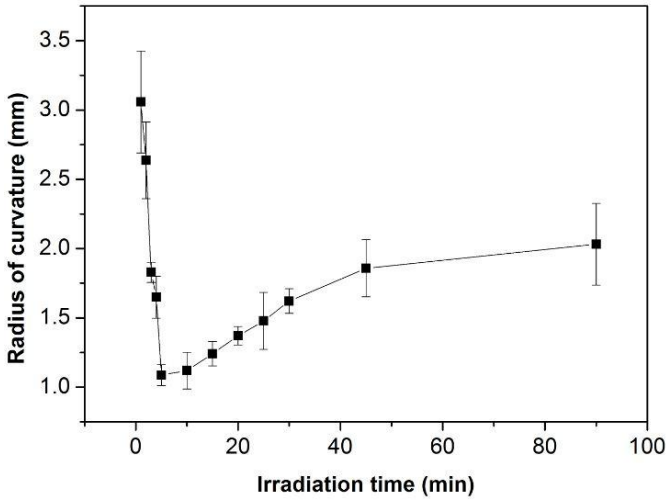

Figure 64. Radius of curvature measured for the optically thick sample as function of irradiation time. The data points are the average of the four segments obtained from a sample and the error bars represent the standard deviation

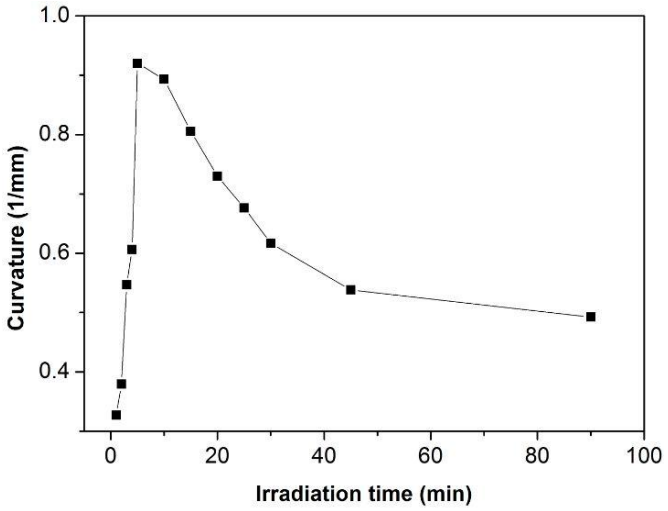

Figure 65. The average values for the sample for the reciprocal of the radius, or curvature as a function of irradiation time

The final parameter used to alter the radius of curvature for the optically thick samples was irradiation intensity. As with the length of irradiation, controlling the intensity of the irradiation affects the depth of irradiation through the thickness of the sample. To illustrate the effect of the intensity of irradiation on the subsequent curvature of the material, each sample was elongated to 10% strain and exposed to varying intensities of irradiation of 365 nm for 5 minutes. Theory predicts that initially the increase in light intensity will produce a higher curvature in the sample due to the increase in initiator activation, however beyond some critical intensity, the increased density of photons hitting the sample activate all of the photoinitiators at the surface of the sample and allow the photons to penetrate deeper into the sample. This increased depth penetration causes a reduction in the curvature because there is less of a difference in the stress states through the thickness.

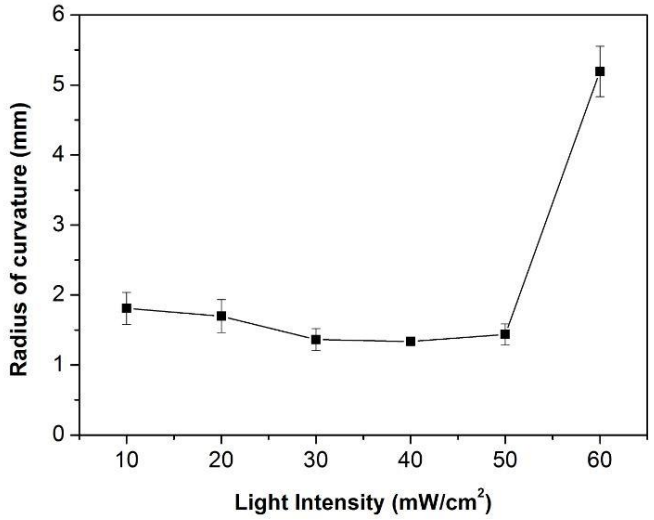

Figure 66. The radius of curvature as a function of light intensity (mW/cm^2). The data points indicate the average values obtained from the sample, and the error bars indicate standard deviation

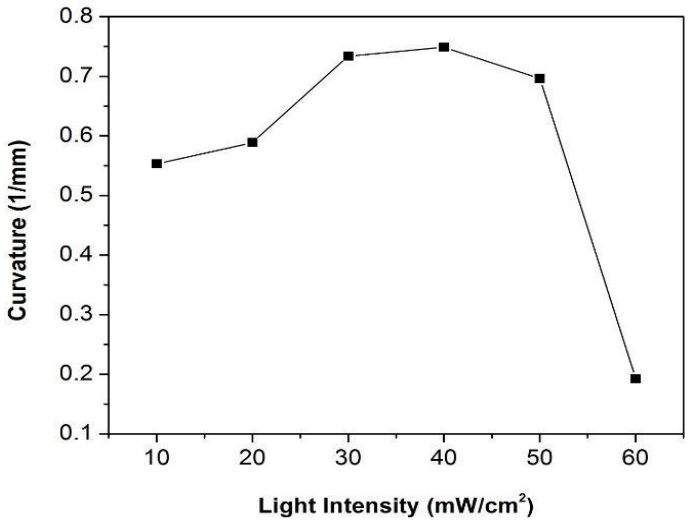

Figure 67. The average values for the reciprocal, or curvature of the optically thick samples as a function of the light intensity (mW/cm^2)

5.7 Hinges

The applied strain as the method of control produced the most consistent and highest degree of curvature. This parameter is also the easiest to control during experimentation. Therefore, the strain-dependence of the induced curvature of the optically thick material was manipulated further to

investigate more controllable structures. The following figures display the curvature as a function of the irradiation width in two ways: constant irradiation width lines with varying applied strain, and constant strain lines with varying the width of irradiation.

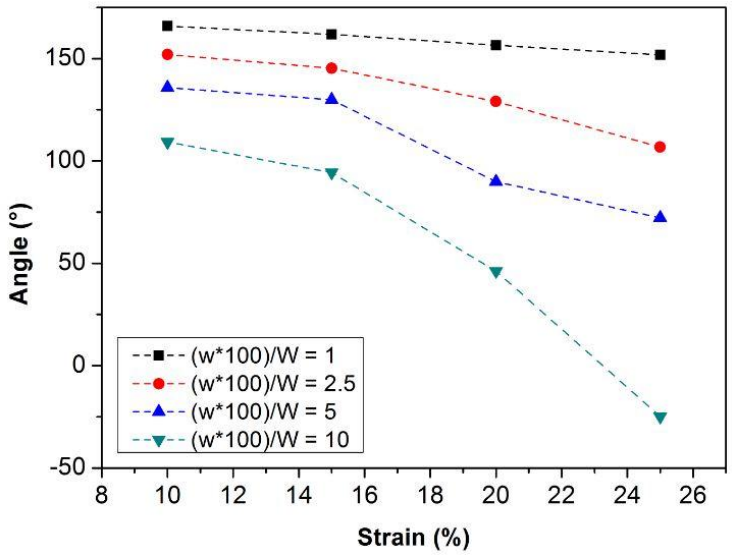

Figure 68. Hinge angle created through irradiation of the optically thick sample through masks of varying the width of the irradiated zone and the applied strain. This curve shows the effect of varying the strain on the four irradiation widths.

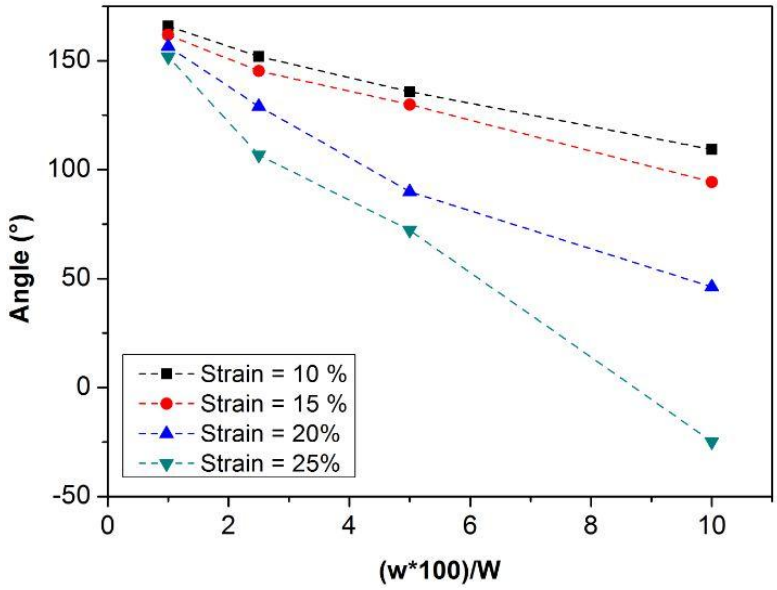

Figure 69. Hinge angle created through irradiation of the optically thick sample through masks of varying the widths of the irradiated zones and the applied strain. This curve shows the effect of varying the mask size for the different values of strain.

Since, of the three parameters (intensity, duration, and strain) strain was used to control the resulting curvature of the localized region, the FEA model that was defined using the strain dependence of the curvature was used the simulate the response of irradiation of localized regions of the optically thick LAP. To measure the effect of the just the width of the irradiated region, the samples were all strained to a value of 20%. Figure 70 shows the comparison between the experimentally obtained samples with the simulated behavior.

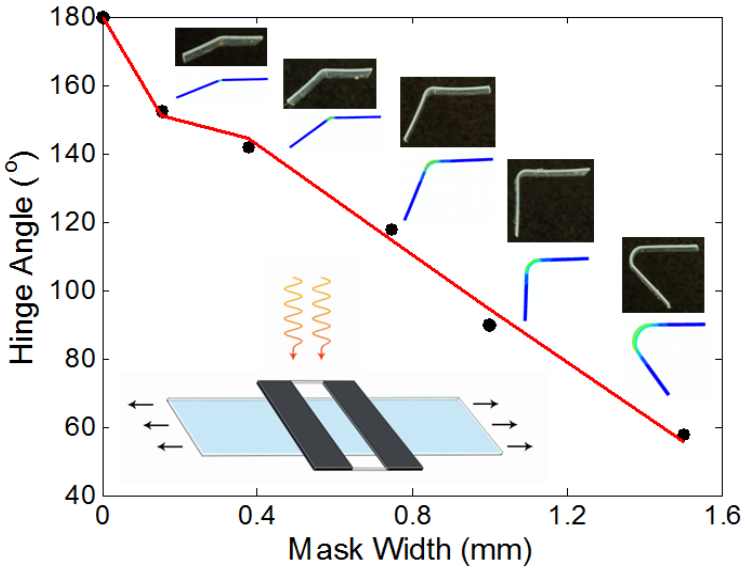

Figure 70. Comparison of the experiment and simulation for the hinge angles as a function of mask width for samples strained to 10%.

The data point at .1mm indicates the limitation of the ability of the unirradiated regions of the sample to compensate for the stress relaxation occurring in the irradiated region.

5.8 Self-Assembling 3D Structures

Building off of the deformation obtained by the curvature and hinge experiments for the optically thick experiments, tests were designed to create structures that would fold up upon the appropriate geometry being cut out of the sheet of material. These structures were irradiated in steps to create localized regions of network reformation to induce a localized deformation to allow the material to "fold up" into a 3D shape upon release of the applied strain. The first self-assembling created to illustrate the localized effects on both sides of the sample as well as showing the different length scales for which the deformation can be controlled. The desired geometry of the heart was a square with sides of length 2 mm with two semicircles on two adjacent edges.

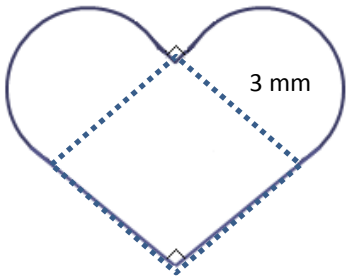

Figure 71. Desired geometry of the "self-assembling" heart shape created with the optically thick LAP by creating a hinge and two semicircles.

To create the 90° hinge, the results of the hinge angle as a function of strain and irradiated width were used. The values of strain that could reasonably obtain a 90° angle were 15%, 20%, and 25%. However, because 25% strain is close to the strain at break, the material cannot consistently achieve this elongation. The required width for using a strain of 15% requires an irradiated region longer than 1.5 mm, which creates a less sharp feature. As a result, the strip was strained to 20% with a 0.75 mm mask to create the center hinge of the heart. The curvature of the semicircles is in the opposite direction of the hinge, so the sample had to be turned over to induce the right shape. To create semicircles with the appropriate radius of curvature, the values obtained from the curvature vs. strain studies was used, and the appropriate value was interpolated. As a result, the sample was strained at 5.5% for 5 min at 40 mW/cm^2.

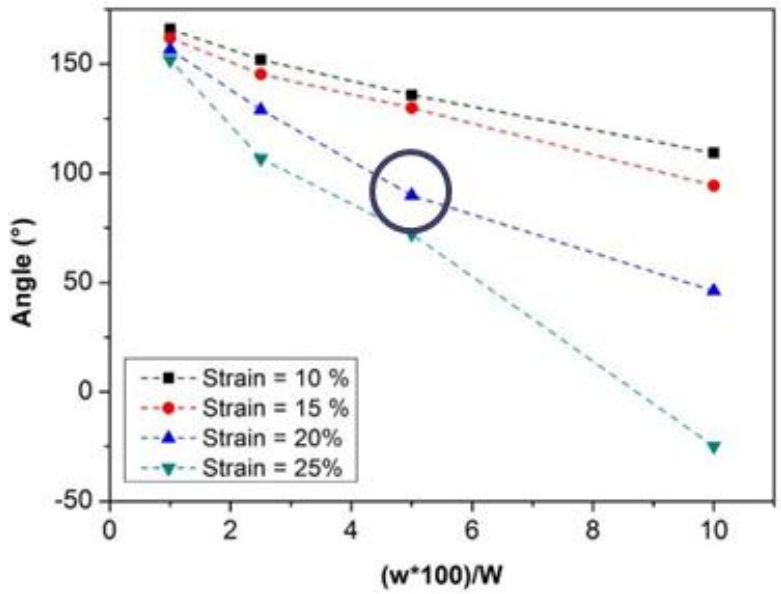

Figure 72. Using the 20% constant strain curve, the width to create a 90 degree angle was chosen using the hinge angle vs. irradiated width presented before

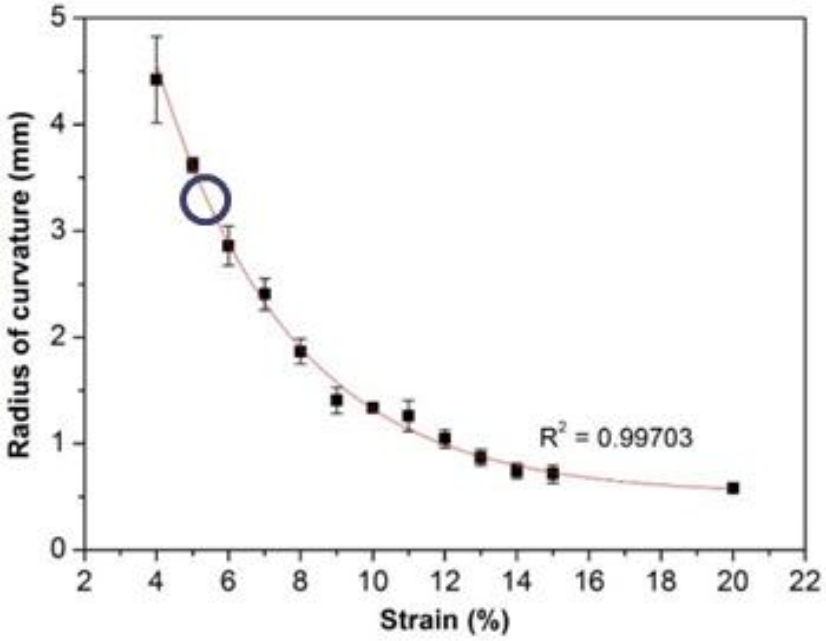

Figure 73. To create the bending behavior a radius of curvature of 3.14 mm was desired. Interpolating on the radius of curvature vs. strain graph, the applied strain of 5.5% was chosen.

Figure 74. Image of the self-assembling heart structure

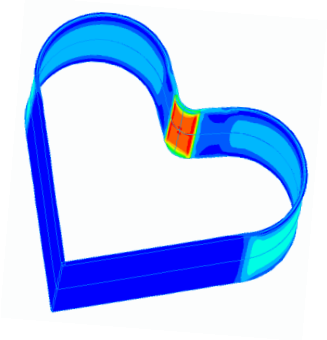

Figure 75. The simulated heart using the same parameters as the experimental protocol

The second self-assembling structure illustrates the anisotropic structure of the material by illustrating the deformation response of the network reformation using different principal directions of strain. This procedure uses the same irradiation procedure for each of five irradiated areas to create five 90 degree hinges that cause a single sheet of the polymer to fold into a cube once appropriately stamped out. The simulation shows that given a procedure that eliminates interference created by irradiating the corners of the base twice, the cube simulated in ABAQUS can attain the same shape that the physical procedure created.

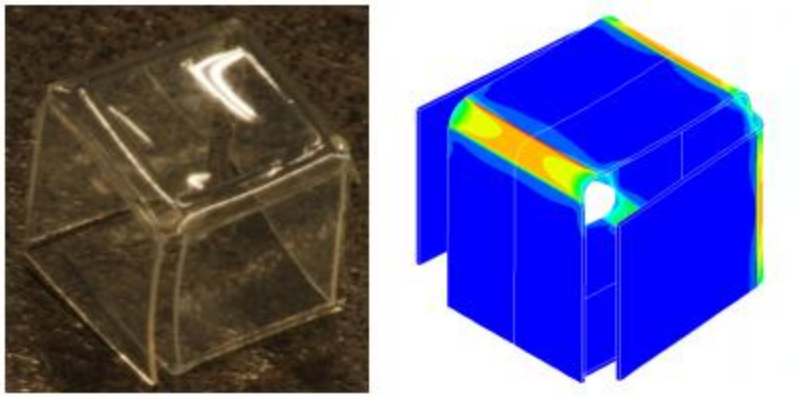

Figure 76. Image of the 5 mm physical box and simulated box

5.9 Improvements

The resolution of the work done here could have been improved through alterations in the chemical and optical set up of the experiment. Chemically, there was uncertainty in the polymerization step from the high reactivity of the vinyl ether. This caused the variability in the time between the start of the polymerization procedure and the irradiation of the gel under the mercury arc lamp with each batch. Using a mechanism that is polymerized through a Michel-addition step instead of using free radical polymerization could eliminate this uncertainty. Optically, the light source and filters used in both the polymerization step and reformation step were not ideal. The collimator at the end of the light guide decreased the deviation of intensity throughout the spot size, but did not completely eliminate it. This effect was on the order of 5% from the middle of the spot size to the outside and was evident in the periodic photopatterning experiments, where there was an increase in the trench depth toward the middle of the spot size. This can be alleviated through a better light collimation system. The filters used had a bandwidth higher than expected. Irradiation through the 365 nm filter in particular resulted in a light that was visible, indicating that the bandwidth of the filter was much larger than stated. This

problem can be alleviated by using a laser light source, which provides an accurate read on the intensity and is a monochromatic light source. Finally, to induce curvature in the LAPs, instead of using UV photoabsorbers that have to potential to create inhomogenous samples, a light source with depth focus can be used to alter the depth of penetration and thereby create a stress relaxation gradient.

6. Conclusions

In this work, studies have been done to characterize and control the behavior of Light Activated Polymers. The type of LAP studied was a network polymer that utilized the Radical-Mediated Addition Chain Transfer (RAFT) mechanism to create macroscale deformation. This was done by first activating free radicals with a controlled light stimulus to initiate the RAFT reaction to create network rearrangement. Since the network rearrangement would preferential arrange the lowest available energy state, when the sample was stressed in any way, the network rearrangement would cause a permanent deformation upon release of the applied strain. This effect was manipulated to prescribe surface patterning on the material. This work not only experimentally showed the ability to create these deformations, but was also used to create and confirm a finite element model that described the deformation behavior of these polymers. For single features, the FEM simulation closely matched the experimental realization. However, for periodic features, there was some disagreement between the model and experiment, indicating that the FEA model is incomplete.

Additionally, the LAP was imparted with some optical thickness through the addition of photoabsorbers. These served to create a gradient for which the material could absorb incident photons. The network rearrangement and subsequent deformation of these materials was controlled in a manner to control out of plane deformation, and even create samples that would self-assemble into prescribed geometries. The tests done with the optically thick samples were also used to create an validate an finite element model that could predict the out of plane deformation behavior of an optically thick sample given experimental parameters.

Through these experimental results, and the comparison of these results to FEM simulations, it is clear that the understanding of the photochemistry controlling the stress relaxation behavior is a good

approximation that can be used to predict and prescribe simple deformations. However, the simulation of the periodic trench case demonstrates that the understanding is incomplete and finer control over the experimental procedure may be needed to reconcile these results.

Modifications to this experimental setup could provide finer control over the deformation and thereby eliminate some of the error associated with the experimental setup. With a collimated light setup with a higher degree of control over the intensity and wavelength of irradiation, the uncertainty of the area of irradiation can be reduced. Furthermore, implementing a light source that has some degree of depth focus can provide control over the depth penetration of light. Improving these areas of the setup will result in an experiment that is a closer approximation to the simulation, and more importantly, a material that can exhibit both surface patterning and bending phenomena without the use of photoabsorbers.

References

[1] E. Hawkes et al., “Programmable matter by folding.,” *Proceedings of the National Academy of Sciences of the United States of America*, vol. 107, no. 28, pp. 12441-5, Jul. 2010.

[2] K. N. Long, T. F. Scott, H. Jerry Qi, C. N. Bowman, and M. L. Dunn, “Photomechanics of light-activated polymers,” *Journal of the Mechanics and Physics of Solids*, vol. 57, no. 7, pp. 1103-1121, Jul. 2009.

[3] M. Niinomi, “Recent research and development in titanium alloys for biomedical applications and healthcare goods,” *Science and Technology of Advanced Materials*, vol. 4, no. 5, pp. 445-454, Sep. 2003.

[4] T. Habijan et al., “The biocompatibility of dense and porous Nickel–Titanium produced by selective laser melting,” *Materials Science and Engineering: C*, vol. 33, no. 1, pp. 419-426, Jan. 2013.

[5] K. Kuribayashi et al., “Self-deployable origami stent grafts as a biomedical application of Ni-rich TiNi shape memory alloy foil,” *Materials Science and Engineering: A*, vol. 419, no. 1–2, pp. 131-137, Mar. 2006.

[6] Y.-hua Li, G.-bin Rao, L.-jian Rong, and Y.-yi Li, “The influence of porosity on corrosion characteristics of porous NiTi alloy in simulated body fluid,” vol. 57, no. December, pp. 448-451, 2002.

[7] G. Wang, Y. Shen, Y. Cao, Q. Yu, and R. Guidoin, “Biocompatibility study of plasma-coated nitinol (NiTi alloy) stents,” no. 6, pp. 102-106, 2007.

[8] T. Namazu, A. Hashizume, and S. Inoue, “Thermomechanical tensile characterization of Ti–Ni shape memory alloy films for design of MEMS actuator,” *Sensors and Actuators A: Physical*, vol. 139, no. 1–2, pp. 178-186, Sep. 2007.

[9] T. F. Scott, R. B. Draughon, and C. N. Bowman, “Actuation in Crosslinked Polymers via Photoinduced Stress Relaxation,” *Advanced Materials*, vol. 18, no. 16, pp. 2128-2132, Aug. 2006.

[10] E. F. Gurnee, “Theory of Orientation and Double Refraction in Polymers,” *Journal of Applied Physics*, vol. 25, no. 10, p. 1232, 1954.

[11] T. M. Conjugated and R. Langer, “Light-induced shape-memory polymers ¨,” vol. 434, no. April, pp. 695-697, 2005.

[12] D. Corbett and M. Warner, “Changing liquid crystal elastomer ordering with light – a route to opto-mechanically responsive materials,” *Liquid Crystals*, vol. 36, no. 10–11, pp. 1263-1280, Nov. 2009.

[13] J. S. Biggins, M. Warner, and K. Bhattacharya, “Elasticity of polydomain liquid crystal elastomers,” *Journal of the Mechanics and Physics of Solids*, vol. 60, no. 4, pp. 573-590, Apr. 2012.

[14] M. Warner and L. Mahadevan, “Photoinduced Deformations of Beams, Plates, and Films,” *Physical Review Letters*, vol. 92, no. 13, pp. 1-4, Apr. 2004.

[15] M. Behl, J. Zotzmann, and A. Lendlein, “Shape-Memory Polymers and Shape-Changing Polymers,” no. November 2009, pp. 1-40, 2010.

[16] W. D. Cook, S. Chausson, F. Chen, L. L. Pluart, C. N. Bowman, and T. F. Scott, “Photopolymerization kinetics , photorheology and photoplasticity of thiol – ene – allylic sulfide networks,” vol. 478, no. April 2007, pp. 469-478, 2008.

[17] M. Yoshida, R. Langer, A. Lendlein, and J. Lahann, “From Advanced Biomedical Coatings to Multi-Functionalized Biomaterials,” *Journal of Macromolecular Science, Part C: Polymer Reviews*, vol. 46, no. 4, pp. 347-375, Dec. 2006.

[18] K. N. Long, M. L. Dunn, T. F. Scott, L. P. Turpin, and H. J. Qi, “Light-induced stress relief to improve flaw tolerance in network polymers,” *Journal of Applied Physics*, vol. 107, no. 5, p. 053519, 2010.

[19] “Stress Relaxation by Addition-fragmentation Chain Transfer in Glassy Polymer Networks A Thesis Submitted to the Faculty of The University of Colorado by Hee Young Park B . S ., Pusan National University , 2000 M . S ., Pusan National University , 2002 In ,” 2011.

[20] B. Myers, M. Bernardi, and J. C. Grossman, “Three-dimensional photovoltaics,” *Applied Physics Letters*, vol. 96, no. 7, p. 071902, 2010.

[21] C. J. Kloxin, T. F. Scott, H. Y. Park, and C. N. Bowman, “Mechanophotopatterning on a photoresponsive elastomer.,” *Advanced materials (Deerfield Beach, Fla.)*, vol. 23, no. 17, pp. 1977-81, May 2011.

[22] T. F. Scott, A. D. Schneider, W. D. Cook, and C. N. Bowman, “Photoinduced plasticity in cross-linked polymers.,” *Science (New York, N.Y.)*, vol. 308, no. 5728, pp. 1615-7, Jun. 2005.

[23] J. F. Quinn, L. Barner, C. Barner-Kowollik, E. Rizzardo, and T. P. Davis, “Reversible Addition−Fragmentation Chain Transfer Polymerization Initiated with Ultraviolet Radiation,” *Macromolecules*, vol. 35, no. 20, pp. 7620-7627, Sep. 2002.

[24] M. Chen, K. P. Ghiggino, A. W. H. Mau, E. Rizzardo, W. H. F. Sasse, and S. H. Thang, “Synthesis of Functionalized RAFT Agents for Light Harvesting Macromolecules,” no. Scheme 3, pp. 5479-5481, 2004.

[25] M. Chen, K. P. Ghiggino, A. W. H. Mau, E. Rizzardo, S. H. Thang, and G. J. Wilson, “Synthesis of light harvesting polymers by RAFT methods.,” *Chemical communications (Cambridge, England)*, vol. 61, no. 19, pp. 2276-7, Oct. 2002.

[26] G. Moad, E. Rizzardo, and S. H. Thang, “Radical addition–fragmentation chemistry in polymer synthesis,” *Polymer*, vol. 49, no. 5, pp. 1079-1131, Mar. 2008.

[27] J. Chiefari et al., “Thiocarbonylthio Compounds (SdC (Z) S-R) in Free Radical Polymerization with Reversible Addition-Fragmentation Chain Transfer (RAFT Polymerization). Effect of the Activating Group Z,” pp. 2273-2283, 2003.

[28] Sigma Aldrich, “Pentaerythritol tetrakis(3-mercaptopropionate) Material Safety Data Sheet,” 2012.

[29] B. Bock, T. Gdmp, and B. Bock, “THIO -CHEMICAL-S Specification / Technical Data Sheet THIO - CHEMICAL-S,” 2012.

[30] R. a. Evans and E. Rizzardo, “Free radical ring-opening polymerization of cyclic allylic sulfides: Liquid monomers with low polymerization volume shrinkage,” *Journal of Polymer Science Part A: Polymer Chemistry*, vol. 39, no. 1, pp. 202-215, Jan. 2001.

[31] C. S. Chemicals and C. E. Segment, “Ciba IRGACURE 819 Ciba IRGACURE 819 Photoinitiator,” pp. 1-3, 2001.

[32] C. S. Chemicals and C. E. Segment, “Ciba IRGACURE 184 Ciba IRGACURE 184 Photoinitiator,” pp. 2-4, 2001.

[33] T. C. C. BASF, “Ciba TINUVIN 5060 Data Sheet,” 2001.

[34] T. C. C. BASF, “Tinuvin 360 Safety Data Sheet,” 2010.

[35] Omnicure, “OmniCure S2000 UV/Vis Spot Curing System,” 2000.

[36] International Light Technologies, “XRD(XRL)340A — International Light Technologies Detector Data.” .

[37] TA Instruments, “TA Instruments Dynamic Mechanical Analyzer.”

[38] Dymek Company Ltd., “Veeco (Dektak) – Stylus Profiler.”

[39] P. J. Flory, “Molecular theory of rubber elasticity,” vol. 20, no. July, pp. 1317-1320, 1979.

[40] J. Blacklock et al., “Cross-linked bioreducible layer-by-layer films for increased cell adhesion and transgene expression.,” *The journal of physical chemistry. B*, vol. 114, no. 16, pp. 5283-91, Apr. 2010.

[41] J. Ryu, M. D’Amato, X. Cui, K. N. Long, H. Jerry Qi, and M. L. Dunn, “Photo-origami—Bending and folding polymers with light,” *Applied Physics Letters*, vol. 100, no. 16, p. 161908, 2012.